Quaternary Science Reviews 344 (2024) 109010



Contents lists available at ScienceDirect

Quaternary Science Reviews

journal homepage: www.elsevier.com/locate/quascirev





Ice-sheet burial and erosion inferred from cosmogenic nuclide bedrock depth profiles: Implications for the glaciation history of northeastern Fennoscandia

Jane L. Andersen [a,b,*], Mads F. Knudsen [a], A.P. Stroeven [b,c], Jesper Olsen [d], Vivi K. Pedersen [a]

[a] Department of Geoscience, Aarhus University, Denmark
[b] Department of Physical Geography, Stockholm University, Sweden
[c] Bolin Centre for Climate Research, Stockholm University, Sweden
[d] Department of Physics and Astronomy, Aarhus University, Denmark

ARTICLE INFO

Handling editor: C. O'Cofaigh

ABSTRACT

In this study, we evaluate the application of shallow (<2.5 m) cosmogenic depth profiles in bedrock to constrain long-term ice-burial and erosion histories. Using Markov Chain Monte Carlo inversion modelling on a series of synthetic scenarios, we demonstrate that cosmogenic ^{10}Be and ^{26}Al profiles provide more robust constraints on ice-burial duration and erosion histories than surface samples alone, particularly when erosion rates are low (<5–10 m Myr^{-1}) and/or non-steady. We apply this method to new depth profiles of ^{10}Be and ^{26}Al measurements from two tors in the Parkajoki region in northeastern Sweden. Our results indicate erosion depths of ~2–10 m and ice burial for ~20–35% of the time since 500 ka. These estimates imply more erosion and less ice burial than previously inferred from the same tors. However, by re-assessing the extent of ice cover during the Weichselian from existing records, we show that some cosmogenic nuclide inheritance predates the penultimate glacial maximum (Late Saalian), implying limited glacial erosion in the Parkajoki region during the last glacial cycle.

1. Introduction

The purpose of this paper is to explore whether cosmogenic nuclides measured in shallow (<2.5 m) bedrock depth profiles can help constrain erosion-rate and ice-sheet histories prior to the Last Glacial Maximum (LGM, ~26-19 ka). This is important because widespread subglacial erosion has removed most glacial and interglacial sediments deposited prior to the LGM in core regions of the large Pleistocene ice sheets (Mangerud, 2004; Olsen et al., 2013; Dalton et al., 2022a), thus limiting more direct evidence of past events. The general scarcity of pre-LGM terrestrial sedimentary archives not only restricts our knowledge of the extent and duration of pre-LGM ice covers, but also our ability to understand the effect of past climate changes on ice-sheet dynamics.

Cosmogenic nuclides accumulate in Earth's near-surface through nuclear reactions with high-energy particles from space known as cosmic radiation (Dunai, 2010). Cosmogenic nuclides are frequently employed to date the timing of last deglaciation under the assumption that the derived exposure ages result from a single period of exposure. However, so-called inherited cosmogenic nuclides that accumulated prior to the LGM often constitute a substantial portion of the total inventory of long-lived cosmogenic nuclides measured in bedrock surfaces at high latitudes (Briner et al., 2014; Jansen et al., 2019); for instance ^{10}Be ($T_{1/2}$: 1.4 Myr; Chmeleff et al., 2010; Korschinek et al., 2010) and ^{26}Al ($T_{1/2}$: 0.7 Myr; Nishiizumi, 2004). These inherited nuclides inhibit the determination of the timing of last deglaciation of a site, but simultaneously record the intertwined signal of exposure and erosion of the bedrock surface prior to the LGM. Bedrock surfaces with inherited nuclides thus provide an opportunity to gauge the pre-LGM ice cover history. Traditionally, multiple cosmogenic nuclides with different half-lives measured in bedrock surfaces have been interpreted in terms of 'minimum-limiting total exposure and ice-burial histories' whereby the differential decay between nuclides is inferred to arise from a period of ice burial following surface exposure (Bierman et al., 1999). However, end-member scenarios of either i) lengthy subaerial exposure followed by episodic erosion of less than a few meters of rock (Fig. 1, Scenario A, blue curves), and ii) no or little subaerial exposure (lengthy ice burial) with slow recent erosion rate (Fig. 1, Scenario B, orange curves), can lead to similar surface inventories of cosmogenic ^{10}Be and ^{26}Al (Bierman et al., 1999; Knudsen and Egholm, 2018). Despite the vastly different ice-burial durations (Fig. 1b; 14% vs 79% ice burial since

* Corresponding author. Department of Physical Geography, Stockholm University, Sweden.
E-mail address: jane.lund.andersen@outlook.com (J.L. Andersen).

https://doi.org/10.1016/j.quascirev.2024.109010
Received 1 July 2024; Received in revised form 3 October 2024; Accepted 14 October 2024
Available online 23 October 2024
0277-3791/© 2024 The Authors. Published by Elsevier Ltd. This is an open access article under the CC BY license (http://creativecommons.org/licenses/by/4.0/).

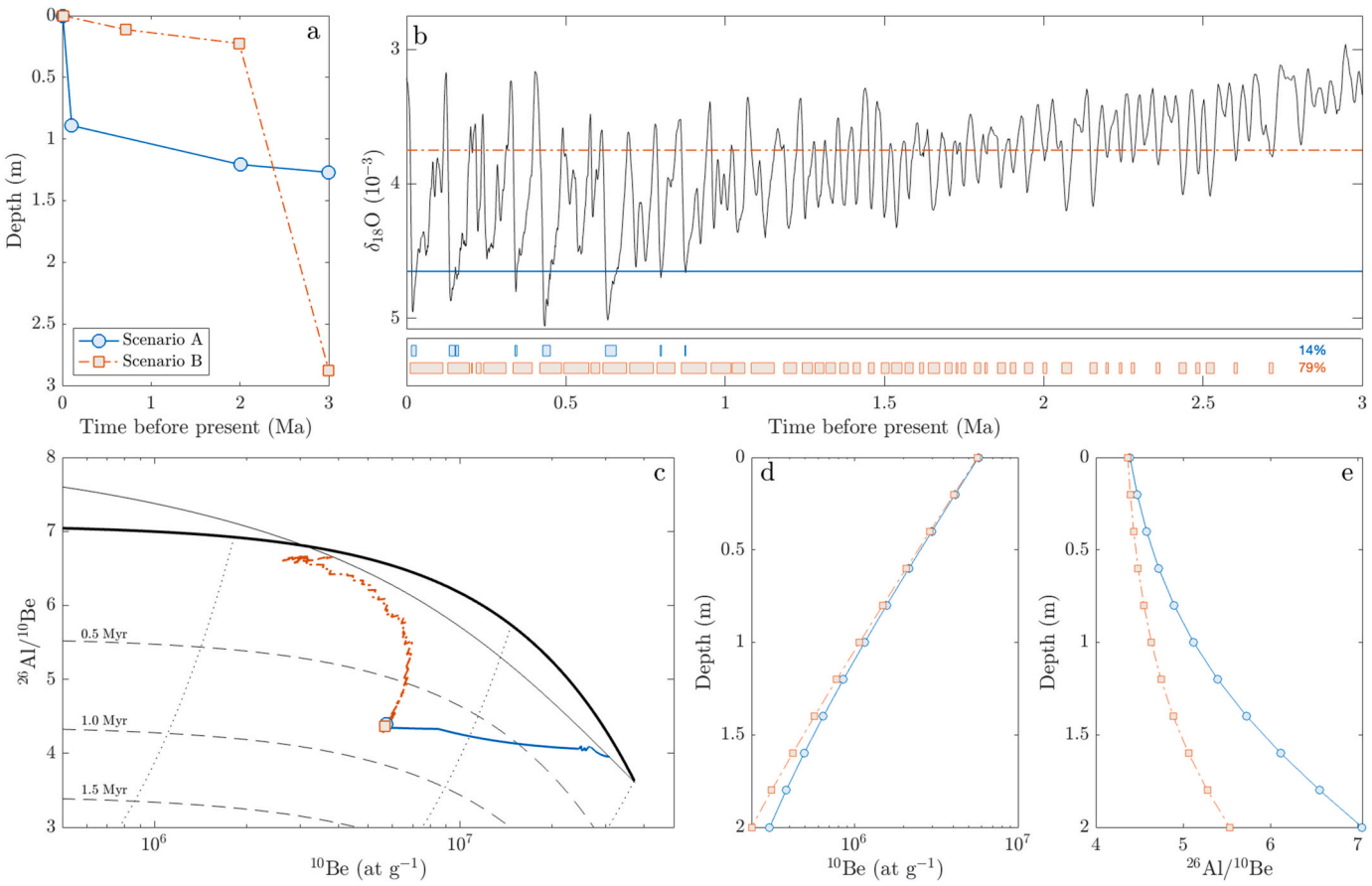


Fig. 1. Illustration of how two end-member surface exposure and erosion scenarios can lead to similar cosmogenic nuclide concentrations in bedrock surfaces. a. Exhumation and b. exposure histories colored by scenario. The black curve in (b) shows the Lisiecki and Raymo (2005) $\delta^{18}O$ stack with 4 kyr smoothing, the horizontal lines indicate the $\delta^{18}O_{th}$ for each scenario and the bars at the bottom indicate the timing and duration of ice-covered periods for the two scenarios with the duration of ice burial since 500 ka indicated in percent. c. Two-nuclide diagram casting $^{26}Al/^{10}Be$ against ^{10}Be with continuous exposure line (thick black line), steady erosion (thin black line), burial paths (black dotted lines), and burial iso-lines with 500 kyr spacing (black dashed lines). The colored lines track the bedrock surface inventories of cosmogenic nuclides for the two scenarios through the last 3 Myr with the markers showing the present-day inventories. e. ^{10}Be and f. $^{26}Al/^{10}Be$ depth profiles at present day.

500 ka), it is not possible to distinguish between these two end-member scenarios based only on measurements of ^{10}Be and ^{26}Al in surface samples, although combining nearby samples with different cosmogenic nuclide inventories may help to uncover the most likely scenario (Knudsen and Egholm, 2018).

In this study, we explore the potential of using shallow bedrock profiles of cosmogenic ^{10}Be and ^{26}Al to constrain ice burial and erosion histories. We first inverse model a set of synthetic scenarios of varying ice burial and erosion histories to study which histories are better resolved with the use of cosmogenic depth profiles (**Section 2**). We then present ^{10}Be and ^{26}Al inventories from two bedrock cores retrieved at a northern Scandinavian study site and assess the glaciation and erosion histories derived from inverse modelling of these new data (**Section 3**). Finally, we discuss the inversion results in the context of the established chronology of glacial events in northeastern Fennoscandia, and address limitations regarding the depth profile inversion approach (**Section 4**).

2. Exploring the usefulness of shallow cosmogenic ^{10}Be and ^{26}Al depth profiles through inversion of synthetic ('known-truth') scenarios

2.1. Inversion approach

To explore the usefulness of shallow cosmogenic ^{10}Be and ^{26}Al depth profiles for constraining long-term exposure and erosion histories of bedrock surfaces, we apply a Markov Chain Monte Carlo (MCMC) inversion approach (Knudsen et al., 2015; Andersen et al., 2020; Skov et al., 2020) to a series of synthetic ('known-truth') scenarios. A successful inversion that pinpoints a true scenario within narrow uncertainty bands, will illustrate the uniqueness, and thus the usefulness, of the cosmogenic nuclide depth profiles to constrain a given scenario.

Our forward model is derived from the one described in Andersen et al. (2020) and Skov et al. (2020), and includes a set of model parameters that control the exposure and exhumation histories of a site (Fig. 2). The exposure history is defined by two parameters: a glaciation threshold ($\delta^{18}O_{th}$) that is applied to a stacked global benthic $\delta^{18}O$ record (Lisiecki and Raymo, 2005) that divides periods of glacial cover (zero production) from periods of surface exposure (Fig. 2a), and the timing of last deglaciation (T_{dg}; Fig. 2b) that is often known locally with some certainty. The exhumation history is defined by an initial steady-state erosion rate (E_0) and a series of modelled time-depth tie points (T_{dg}, T_2, T_3, Z_{dg}, Z_2, Z_3) where Z_{dg} represents the depth of the sample at the last deglaciation (Fig. 2b). The MCMC inversion approach generates thousands of forward models to explore different combinations of exposure and exhumation, and map out the distribution of these parameters that result in cosmogenic nuclide concentrations matching the measured (or synthetic) concentrations. Because of inherent trade-offs between single parameter values constraining the exhumation path, we report the derived parameters 'time of 1 m erosion' and 'erosion since 500 ka' to characterize sample trajectories, as samples within the depth

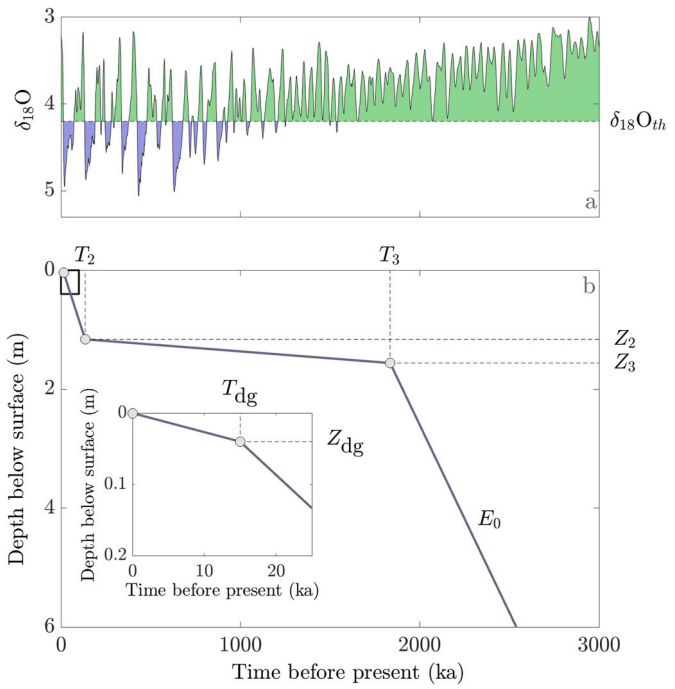


Fig. 2. Schematic of the forward model parameters. Schematic illustrating the eight model parameters. a) The exposure histories are defined from a stacked global benthic $\delta^{18}O$ record (Lisiecki and Raymo, 2005) in combination with a modelled glaciation threshold parameter ($\delta^{18}O_{th}$), dividing periods of glacial cover (blue) from periods of surface exposure (green). b) The exhumation histories are parameterized using a series of modelled time-depth tie points (T_{dg}, T_2, T_3, Z_{dg}, Z_2, Z_3). The inset shows expanded scale around timing of last deglaciation (T_{dg}) and the corresponding depth (Z_{dg}). The final model parameter (E_0) is a constant erosion rate determining the exhumation path from the initiation of each model run at 3 Ma until T_3. Figure modified from Andersen et al. (2020).

profile are exhumed to their present position through surface erosion. Likewise, we report the exposure history as 'ice burial since 500 ka (%)'. For the inversions performed in this study, the inversion algorithm was allowed to explore i) $\delta^{18}O_{th}$ values between 3.5 and 5.0 ‰ corresponding to ice burial durations of about 1–90% since 500 ka, ii) Z_{dg} values between 0 and 5 cm, and iii) a combination of time-depth tie points corresponding to erosion rates anywhere between 0 and 2000 m Myr^{-1}. We used 10 random walkers and continue the search of the parameter space until 100,000 models were accepted per walker for a total of one million accepted models per inversion.

We compute site-specific spallation production rates for ^{10}Be and ^{26}Al in quartz scaled for latitude and elevation according to the 'St' scaling scheme (Stone, 2000), with sea-level high-latitude reference production rates of 4.01 atoms (g quartz)$^{-1}$ yr^{-1} for ^{10}Be and 27.93 atoms (g quartz)$^{-1}$ yr^{-1} for ^{26}Al (Borchers et al., 2016). We compute parameters for ^{10}Be and ^{26}Al production by muon interactions by fitting three exponentials to the 'model 1A' nuclide-specific, site-atmospheric-pressure dependent muon production profile (Balco, 2017).

2.2. Inversion of synthetic scenarios

We use a set of distinct erosion and exposure histories to test how well cosmogenic nuclide depth profiles can constrain these known erosion and exposure histories. We do this by exploring four different exhumation histories in combination with four different exposure histories, resulting in a total of 16 scenarios (Figs. 3 and 4; Supp. Table S1). The exhumation histories are selected to include both relatively fast and slow, as well as steady and time-variant (episodic) erosion (Fig. 3). The exposure histories span from limited burial under ice (~10% of time since 500 ka) to extensive burial (~75% of time since 500 ka). For each scenario we calculate the ^{10}Be and ^{26}Al depth profiles at present based on the pre-defined exhumation and exposure history. We estimate the expected analytical errors related to the calculated nuclide inventories by interpolating a radioactive to stable nuclide ($^{10}Be/^{9}Be$ and $^{26}Al/^{27}Al$) vs. error curve derived from the distribution of samples measured between 2017 and 2019 at the Aarhus AMS Centre (Supp. Fig. S1), and assuming 10 g clean quartz per sample, 250 µg of ^{9}Be carrier, and a total Al content of 1200 µg. However, we set the minimum analytical error of both ^{26}Al and ^{10}Be to 2.5% to reflect the standard deviation on repeat measurements of the CoQtz-N intercomparison material (Binnie et al., 2019; $n_{10Be} = 31$, $n_{26Al} = 16$) run with samples in the Aarhus lab between 2017 and 2023. For each scenario, we run two inversions; i) one that is constrained by a sample at 0 m depth ('surface sample inversion'), and ii) one that that is constrained by a profile with 6 samples evenly distributed between 0 and 2 m depth ('depth profile inversion'). For the synthetic models the inversion algorithm was allowed to explore time of last deglaciation (T_{dg}) values between 10 and 20 ka.

2.2.1. Results of synthetic inversions

The four inversion results that share a true 'ice burial since 500 ka' value of ~25 % but represent four distinct exhumation scenarios, demonstrate that the depth profile inversions provide a better fit to the true exposure and exhumation histories than the surface sample inversions for all four exhumation patterns (Fig. 3). This is reflected in narrower distributions of both exhumation paths and the 'ice burial since 500 ka (%)' parameter, and that the highest density of accepted model solutions are generally centered on the true histories. For the depth-profile inversions, the fit to the true values is generally better for scenarios with relatively low erosion rates (Fig. 3a and b) than for higher erosion rates (Fig. 3c and d), especially regarding the 'ice burial since 500 ka (%)' parameter. It is also clear that including samples at depth enables the inversion algorithm to closely fit the true exhumation and exposure history even when a rapid erosion event follows a long period of slow erosion, a scenario that is almost entirely unconstrained by the surface sample inversion (Fig. 3b).

Inverting a depth profile resolves the true ice-sheet burial histories better also for other ice-burial durations (~10%, ~50% and ~75% of 'ice burial since 500 ka'), although for lower ice-burial durations the full ranges of accepted parameter values are sometimes wider (Fig. 4, top rows). In two cases (scenarios 5 and 6), the highest density of accepted model solutions are offset from the true values, displaying a slight skew towards more ice burial. The inclusion of depth samples also generally improves the fit to the true exhumation history assessed through the 'Time of 1 m erosion' and 'Erosion since 500 ka' parameters (Fig. 4, middle and bottom rows), although the improvement from using a depth profile over a surface sample is relatively modest for some scenarios (e.g., scenarios 1 and 2). For the scenarios with faster erosion (Fig. 4; Supp. Fig. S2-S4), both inversions (surface sample and depth profile) tend to underestimate the 'erosion since 500 ka' parameter, especially for scenarios with a 'recent' shift to slower erosion (scenarios 13–16; Fig. 4).

2.3. Summary of synthetic inversion exercise

To summarize, inversions of depth profiles generally lead to improved fits to the true exhumation and exposure histories compared to inversions based on surface samples alone. The improvement-of-fit is highest when the samples have experienced long near-surface residence times (i.e., when erosion rates are <5–10 m Myr^{-1}), and our synthetic tests indicate that the exhumation and exposure histories can be resolved even when relatively rapid erosion (< a few meters depth) has taken place within the last few glacial cycles. The latter is important for polar regions where slow subaerial weathering over millions of years may have primed bedrock for episodic glacial erosion during the large late Pleistocene glaciations (Margreth et al., 2016).

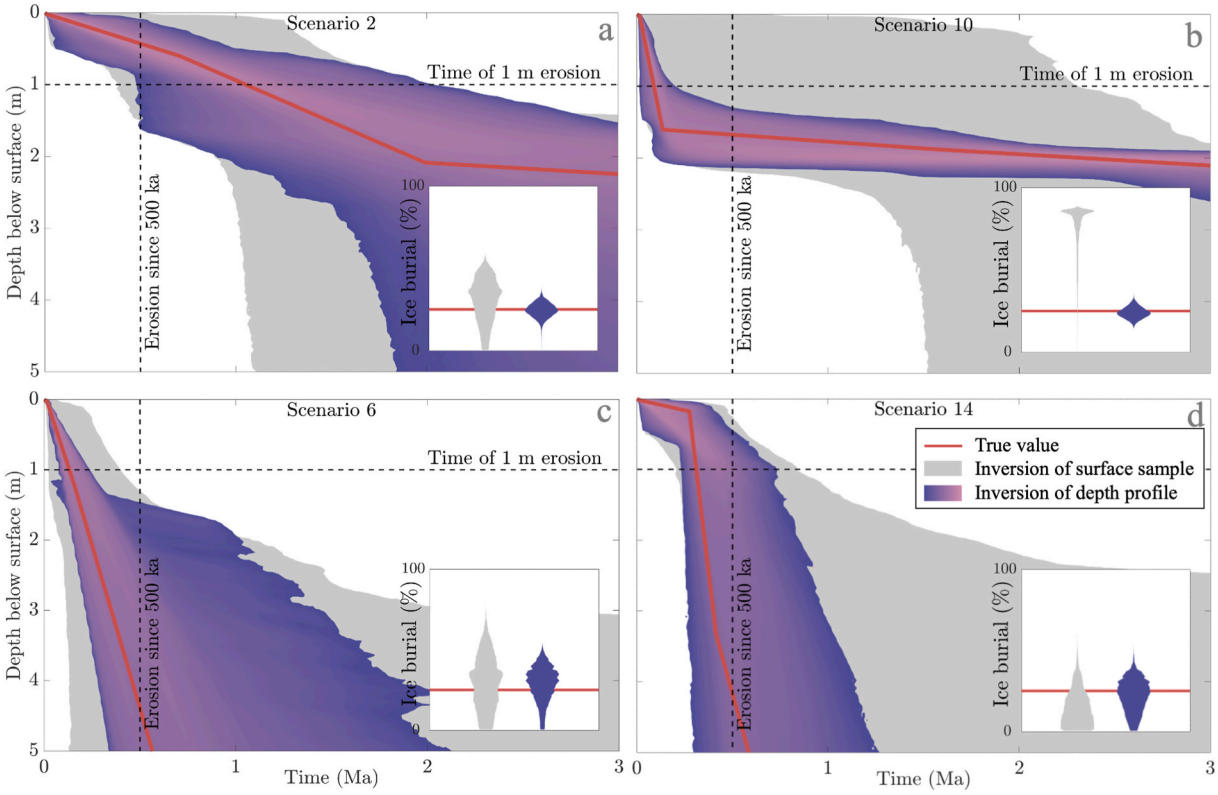


Fig. 3. Exhumation and ice burial for four synthetic exhumation scenario examples, selected to include both relatively slow (a,b) and fast (c,d), as well as steady (a,c) and time-variant/episodic (b,d) erosion. Main plots show true values (red lines), inversion of surface sample (grey patch) and depth profile of 6 depth points down to 2 m depth (blue-pink patch with pink colors indicating a higher frequency of accepted models). Note that the modelled exhumation paths extend to 20 m depth, but that for visibility only the top 5 m are shown here. Insets show the distribution of the derived parameter 'Ice burial since 500 ka (%)' for all accepted models for surface sample inversion (grey patch) and depth profile inversion (blue patch) with true value in red. All four scenarios experience ice burial for ~25% of time since 500 ka. Remaining scenarios with different ice-burial durations are shown in Supplementary Figs. S2-S4.

3. Study site, sample collection and analysis, and inverse model results

To test the use of cosmogenic nuclide depth profiles to constrain ice burial and erosion in the 'real' world, we collected two bedrock drill cores in the Parkajoki region in northern Scandinavia (Figs. 5 and 6). We chose locations where existing surface data indicate cosmogenic nuclide inheritance from pre-LGM exposure, and for logistical reasons selected sites that were accessible within a relatively short walking distance from a road. In the following, we briefly summarize the long-term landscape evolution and glaciation history inferred from the regional geomorphology and published cosmogenic nuclide chronometry. All apparent exposure ages discussed in the text are (re-)calibrated using the LSDn scaling scheme (Lifton et al., 2014) and the global production calibration (Borchers et al., 2016). A regional production calibration exists only for ^{10}Be (Stroeven et al., 2015) which would yield ~4% lower production rates and equivalently higher ages. Due to the lack of an equivalent regional ^{26}Al production calibration, we do not discuss this alternative production calibration further.

3.1. Parkajoki: Naakakarhakka and Lamuvaara tors

Parkajoki is an area around the Parkajoki river in northeastern Sweden on the border with Finland (Fig. 6). The Parkajoki landscape is characterized by a relatively low (150–400 m a.s.l.) and undulating bedrock relief with scattered, tor-dotted hills (Fig. 6; Hättestrand and Stroeven, 2002). Despite the location near the centre of the Scandinavian Ice Sheet (SIS) during the LGM (Fig. 5), the glacial imprint on the landscape is limited to lateral and proglacial meltwater channels and patches of thin till, while landforms indicative of thawed bed conditions and subglacial sliding (fluting, drumlins, striations) are absent (Hättestrand and Stroeven, 2002; Ebert et al., 2015). This contrasts with adjacent regions at similar elevation and with a similar ice burial history that bear imprints of subglacial and glaciofluvial erosion and deposition (e.g., drumlins, fluting, eskers) from different glacial stages as evidenced by cross-cutting relationships of landforms formed during ice-sheet advance and retreat (Kleman, 1992; Kleman et al., 1997; Hättestrand and Stroeven, 2002; Ebert et al., 2015).

In Parkajoki, weathered tors (bedrock knobs) extending below grus mantles typically occur on gneissic or gneissic-granitic hill summits (Hättestrand and Stroeven, 2002). The tors are suggested to constitute remnants of preglacial landscape features (Hättestrand and Stroeven, 2002). If so, they would be indicative of highly inefficient glacial erosion, implying that non-erosive ice established repeatedly and consistently during all Pleistocene glaciations in this region (Hättestrand and Stroeven, 2002; Stroeven et al., 2002). Indeed, the geomorphological contrast between the Parkajoki area and adjacent regions in northern Sweden and Finland, and the inferred contrast in glacial erosion rates has been suggested to imply that all large Fennoscandian glaciations had a similar ice-sheet evolution as the LGM glaciation, repeatedly establishing a divergent and/or cold-based ice flow in the Parkajoki area during phases of both ice-sheet expansion and demise (Hättestrand and Stroeven, 2002).

Cosmogenic nuclide chronometry has been used to test the hypothesis of limited glacial erosion during Pleistocene glaciations in the Parkajoki area. *In situ* cosmogenic ^{10}Be and ^{26}Al dating of surface samples from three tors (Fig. 6; Stroeven et al., 2002) yielded apparent ^{10}Be exposure ages between 37.7 ± 3.4 (2.5) kyr and 79.4 ± 6.4 (4.3) kyr (recalculated in this study, errors: ± total (analytical) uncertainty) and ^{26}Al/^{10}Be ratios from 5.9 ± 0.1 to 6.3 ± 0.1 (Supp. Table S2). A few

different models were applied to these data. Based on a single one-stage exposure-burial scenario, a maximum erosion rate of 1.6 m Ma^{-1} and a minimum total history of 335 ka were suggested, with ice burial estimated to occur during 257 ka (77%) of this time (Stroeven et al., 2002). Stroeven et al. (2002) further calculated a minimum total history of 605 ka based on the assumption that the Parkajoki area was always ice covered when $\delta^{18}O$-values on marine benthic foraminifera exceeded a critical threshold (3.7‰ in the DSDP 607 record; Raymo et al., 1989; Ruddiman et al., 1989). This corresponds to ice burial for approximately 73% of this period. While this analysis implies that the Parkajoki tors survived several extended periods of ice-sheet burial, the data do not dictate that the tors survived from preglacial times. Four additional tor samples from the Parkajoki area yielded apparent ^{10}Be and ^{26}Al exposure ages between 37.7 ± 2.5 (3.4) and 74.4 ± 5.0 (2.3) kyr, with $^{26}Al/^{10}Be$ ratios varying from 5.3 to 6.9 (Supp. Table S2; Stroeven et al., 2006; Li et al., 2008; supplement to Stroeven et al., 2016) in alignment with the conclusions of Stroeven et al. (2002).

Nearby inventories of meteoric ^{10}Be in two pit profiles of grussy saprolite overlain by Weichselian till (Fig. 6) also clearly exceed what could have accumulated since the last deglaciation (Ebert et al., 2012). However, unknown meteoric ^{10}Be concentrations prior to glaciation inhibits precise age determination of the saprolite with inferences ranging between 0.8 and 5 Ma (Ebert et al., 2012). While these pit profiles support the conclusion that recent ice sheets in the Parkajoki area were mostly cold-based and non-erosive, they do not provide conclusive evidence that the Parkajoki tors survived all Quaternary glaciations.

Here, we revisit two of the previously sampled tors in the Parkajoki area with highest cosmogenic nuclide concentrations in their bedrock surfaces, namely Naakakarhakka and Lamuvaara (Fig. 6). Our aim is to test whether cosmogenic depth profiles can help to improve the existing constraints on the long-term ice-sheet burial and erosion history of this region.

3.2. Sampling, cosmogenic nuclide analyses and results

We collected two 5-cm diameter bedrock cores to depths of 180 cm (Naakakarhakka) and 201 cm (Lamuvaara) using a portable backpack drill and analyzed cosmogenic ^{10}Be and ^{26}Al at 7–9 depths within each profile, including at the surface (Fig. 7; Supp. Tables S3-S5). The cores were divided into ~5 cm thick slices that were crushed before quartz was separated from the 250–500 μm sieved fraction using froth flotation, magnetic separation, and HF leaching (Child et al., 2000; Kohl and Nishiizumi, 1992). Be and Al were isolated from the dissolved quartz by ion chromatography and pressed into targets for $^{26}Al/^{27}Al$ and $^{10}Be/^{9}Be$ analysis at the Aarhus AMS Centre following methods described in Andersen et al. (2020). An aliquot of the dissolved quartz was analyzed for total Al content by inductively coupled plasma optical emission spectrometry (ICP-OES) at The University of Bergen. With each batch of samples (n = 2), we prepared and analyzed an aliquot of the CoQtz-N intercomparison material (Binnie et al., 2019). Analytical uncertainties were propagated in quadrature but set to a minimum of 2.5% for both ^{10}Be and ^{26}Al to reflect the reproducibility of measurements on laboratory intercomparison material at Aarhus University (**See Section 2.2**).

As expected, ^{10}Be and ^{26}Al inventories decrease systematically with increasing depth below the surface (Fig. 7). For Naakakarhakka, ^{10}Be concentrations vary from 48.3 ± 0.8 × 10^4 at g^{-1} at the surface to 5.0 ± 0.3 × 10^4 at g^{-1} at 175–180 cm depth and corresponding ^{26}Al concentrations vary from 322 ± 6 × 10^4 at g^{-1} to 37 ± 22 × 10^4 at g^{-1} (Fig. 7; Supp. Table S5). For Lamuvaara, ^{10}Be concentrations vary from 33.7 ± 1.1 × 10^4 at g^{-1} at the surface to 3.4 ± 0.1 × 10^4 at g^{-1} at 190–201 cm depth and corresponding ^{26}Al concentrations vary from 242 ± 5 × 10^4 at g^{-1} to 21 ± 1 × 10^4 at g^{-1} (Fig. 7; Supp. Table S5). All $^{26}Al/^{10}Be$ ratios overlap within 2σ with a mean value of 6.8 ± 0.3 (1SD). The CoQtz-N material analyzed together with each batch of samples yielded ^{10}Be concentrations of 2.49 ± 0.05 × 10^6 at g^{-1} and 2.49 ± 0.04 × 10^6 at g^{-1} and ^{26}Al concentrations of 16.2 ± 0.3 × 10^6 at g^{-1} and 16.5 ± 0.2 × 10^6 at g^{-1} (Supp. Table S6; Supp. Fig. S5), which overlap within 1σ of each other and with the preliminary consensus value for ^{10}Be of 2.53 ± 0.09 × 10^6 at g^{-1} and ^{26}Al of 15.6 ± 1.6 × 10^6 at g^{-1} (Binnie et al., 2019), adding confidence to the robustness of our results.

3.3. Inversion of Parkajoki depth profiles

To explore the exposure and erosion histories that may explain the measured cosmogenic nuclide inventories we apply the MCMC inversion approach described above to our depth profiles and compare to inversions based solely on the surface samples of each tor. We inverse model each core depth profile individually, but also perform a joint inversion of both profiles in a setup where the ice-sheet burial history is tied together for the two sites while the erosion histories are allowed to vary independently for each site. The assumption of similar overall ice-sheet histories for the two sites is justified by the close vicinity and elevations of the core sites (~5 km and 45 m, respectively), while erosion can vary locally over small distances. The inversion algorithm was allowed to explore time of last deglaciation (T_{dg}) values between 9 and 13 ka, a conservative interval around the reconstructed time of last deglaciation (c. 11-10 ka; see section 3.4.1.1).

Individual inversions of the bedrock depth profiles show that both sites experienced very similar erosion histories with 1 m of erosion since 0.13–0.28 Ma (Naakakarhakka) and 0.10–0.27 Ma (Lamuvaara), and erosion depths of ~2–10 m since 500 ka for both sites (Fig. 8; Supp. Table S7; 2.5–97.5% range of accepted models). As such, the erosion histories for these sites approximate the high-erosion scenarios from our synthetic inversion experiments (Scenarios 5–8 or 13–16; Fig. 3c–d, 4). The joint inversion of both depth profiles leads to slightly modified erosional histories with 1 m of erosion since 0.15–0.29 Ma (Naakakarhakka) and 0.11–0.23 Ma (Lamuvaara), and erosion since 500 ka exceeding 1.7 m (Naakakarhakka) and 2.2 m (Lamuvaara; Fig. 8; Supp. Table S7; 2.5–97.5% range of accepted models).

Although the range of potential ice-burial histories narrows by including samples at depth compared to a surface sample alone, the 'Ice burial since 500 ka' parameter remains relatively poorly constrained for the depth profile inversions at both sites (Fig. 8; Supp. Table S7). For the individual inversions the ice-burial durations are between 2.4 and 39.3% (Naakakarhakka) and 6.2–54.0% (Lamuvaara) of time since 500 ka, while the joint inversion indicates ice burial of both sites for 12.8–40.7% of time since 500 ka (2.5–97.5% range of accepted models). The results of the joined inversion are most closely reminiscent of our synthetic scenarios 6 and 14 (Fig. 3c–d, 4). We know from the synthetic scenario inversions that the distribution of the 'ice-burial duration since 500 ka' parameter tends to skew towards more ice burial for true ice burial durations ~10–25% of time when erosion is relatively high (scenarios 5 and 6; Fig. 4). We therefore estimate that the true ice-burial duration is close to the peak of accepted solutions (~30%), or slightly below it, indicating that the Parkajoki region experienced ice-sheet burial around ~20–35% of time since 500 ka (Fig. 8).

We note that the Naakakarhakka and Lamuvaara core profiles were not collected from flat bedrock surfaces, but from tors protruding the surrounding landscape. This means that a component of the cosmogenic nuclide inventories in our depth profiles could stem from lateral production through the sides of the tors, and that our forward model therefore underestimates the total cosmogenic production profile. However, we collected our core profiles as far from any vertical edges on the tors as feasible (>1–1.5 m) and we therefore estimate that this effect is of minor importance (generally <2–3% of production).

3.4. Test of simple scenario: deep erosion during the penultimate glacial maximum

Eemian deposits and tills assumed to originate from the penultimate

glacial period (Saalian/MIS 6) typically lie directly on bedrock in Sweden (Robertsson, 1997) and Finland (Lunkka et al., 2015; Plikk et al., 2016). Indeed, to our knowledge, there is little, if any, stratigraphic or chronometric evidence for pre-Saalian deposits. This could indicate that the SIS eroded most pre-existing deposits during the penultimate glacial maximum. Given this, we evaluate whether the exposure history recorded by the Parkajoki tors could entirely post-date the penultimate glacial maximum (i.e. <130 ka). Specifically, we test a simple scenario where erosion during the penultimate glaciation removed any previously accumulated cosmogenic nuclides in tor bedrock surfaces and explore if such a scenario could be consistent with the measured inventories of cosmogenic ^{10}Be and ^{26}Al. To consider the post-Saalian exposure history at Parkajoki, we first review the available Holocene, Weichselian, and Eemian ice-sheet records and reconstructions from northeastern Fennoscandia (**section 3.4.1**). We then apply these suggested exposure histories to evaluate whether inherited nuclides from exposure prior to the Saalian are required to explain the cosmogenic nuclide inventories in the measured depth profiles (**section 3.4.2**).

3.4.1. Post-Saalian exposure of NE Fennoscandia

3.4.1.1. Holocene exposure. Regional reconstructions based on databases of radiocarbon, optically-stimulated luminescence (OSL), thermoluminescence, and cosmogenic nuclide deglaciation ages agree that the deglaciation of the Parkajoki area following the LGM took place between 11 and 10 ka, most likely close to 10.1 ka (Hughes et al., 2016; Stroeven et al., 2016). The nearest ^{14}C dates from the Aareavaara site 30 km SSW of Parkajoki (included in the databases) indicate deglaciation ~10.7 cal yr BP (Möller et al., 2013b, Fig. 6). For our simple scenario, we therefore infer full exposure for a minimum of 10 kyr between 10 and 0 ka, and a maximum of 11 kyr between 11 and 0 ka (Fig. 9a).

3.4.1.2. Middle and late Weichselian exposure. In the Middle Weichselian, a growing body of evidence suggest that the SIS was restricted to the spine of the Scandes during most of MIS 3 – the period leading up to the LGM (Möller et al., 2013a; Helmens, 2014; Kleman et al., 2021; Alexanderson et al., 2022; Dalton et al., 2022b; Mangerud et al., 2023). At Hannukainen, 35 km east of Parkajoki in northwestern Finland (Fig. 6), OSL dating from a stratigraphic section indicate ice-free conditions from 55 to 35 ka, followed by a readvance after 35 ka and a second ice-free phase of unknown duration before build-up to the LGM glaciation (Salonen et al., 2014). At Rauvospakka, Kortejärvi, Sainjärvi, and Outojärvi, located 20–40 km west and southwest of Parkajoki (Fig. 6), OSL and ^{14}C dating places the formation of the prominent Lainio Arc section of the Veiki Moraine during an Early MIS 3 advance (Fig. 5; Alexanderson et al., 2022). The suggested age of formation is around 56.5–54.2 ka, preceeded by retreat of the ice margin west of the Veiki moraine (and thereby west of Parkajoki) during Greenland Interstadial 16.1 from 58 to 56.5 ka (Alexanderson et al., 2022). Radiocarbon dates from kettlehole sediments in the nearby Riipiharju esker (Fig. 6) are likewise coherent with an early MIS 3 exposure of the region (Hättestrand and Robertsson, 2010). A major deglaciation of Scandinavia during MIS 3 is consistent with data from Finland (Ukkonen et al., 1999; Mäkinen, 2005; Alexanderson et al., 2008; Helmens et al., 2009; Sarala et al., 2016), central and southern Sweden (Alexanderson et al., 2010; Möller et al., 2013a; Kleman et al., 2021) and Norway (Mangerud et al., 2023), and also corresponds with ice-sheet demise inferred from global sea-level records (Siddall et al., 2008). The ice-sheet re-advance leading up to the LGM is estimated to occur around 35-30 ka in northern Sweden (Lainio Arc, Alexanderson et al., 2022), which is consistent with ages from central Sweden (Pilgrimstad, Alexanderson et al. (2010); Kleman et al., 2020; Fig. 5), as well as far-field records indicating a global sea-level drop from ~35 ka (Winograd, 2001; Farmer et al., 2023). Some Finnish records even indicate that the final ice advance leading up to the LGM could post-date 25 ka (Ukkonen et al., 1999; Sarala et al., 2010; Johansson et al., 2011; Salonen et al., 2014). In our simple scenario, we therefore infer full exposure of our sample sites during MIS 3 for a minimum of 21.5 kyr and a maximum of 33 kyr between ~58.0 and 56.5 ka and ~35-25 ka (Fig. 9a).

3.4.1.3. Early Weichselian exposure. In the Early Weichselian, the duration(s) of ice-free period(s) are not constrained in the immediate vicinity of Parkajoki, although one or two ice-free period(s), pre-dating MIS 3, is recorded in the Riipiharju esker deposits (Fig. 6; Hättestrand and Robertsson, 2010). In north-eastern Fennoscandia, the Early Weichselian is characterized by two long, mild, and forested periods (MIS 5c and 5a) that are interrupted by two short, relatively cold, and dry intervals (MIS 5d and 5b) associated with mountain-centered ice sheets (Helmens, 2014). Regional reconstructions suggest that Parkajoki was exposed during MIS 5a and 5c, and ice covered during MIS 5b and 5d (Batchelor et al., 2019). Indeed, based on climatic reconstructions, it is likely that small ice remnants restricted to the mountains characterized glaciation during MIS 5a and MIS 5c (Väliranta et al., 2009; Mangerud et al., 2011; Helmens, 2014; Batchelor et al., 2019). It is less clear how far the ice sheet advanced eastwards during the two stadial periods (MIS 5d and 5b) and for how long it occupied such extended positions.

Records from Finland provide some constraints on the Early Weichselian ice sheet history. Six distinct till units have been identified in northern Finland (Johansson et al., 2011). Originally, the oldest units in northern Finland were thought to pre-date the Saalian (Hirvas, 1995), but OSL dating near Rautuvaara (~35 km W-SW of Parkajoki; Fig. 6) later demonstrated that the entire sediment succession, including five till beds, was deposited during the Weichselian, with only the lowest till bed correlated to the Early Weichselian (Lunkka et al., 2015) although it could also be older (Salonen et al., 2014). The most complete record of Early Weichselian glaciations in northeastern Fennoscandia derives from Sokli (Fig. 5; Helmens et al., 2000). It shows that the ice sheet did not extend to eastern Finland during MIS 5d. Instead of a MIS 5d till unit, a silt unit containing a tundra-type pollen assemblage separates MIS 5e from 5c. On the contrary, Sokli was glaciated during MIS 5b, when the ice sheet deposited a till bed. Early Weichselian ice-free conditions at Sokli have been dated to around 94 ka (MIS 5c) and 74–80 ka (MIS 5a) and are associated with deposition of fossil-rich fine-grained (mostly lacustrine) sediments (Helmens et al., 2000; Alexanderson et al., 2008). These dates constrain the duration of the MIS 5b glacial advance at Sokli to <14 kyr.

Several end-moraine complexes extend across northern Finland in a NE-SW direction (Fig. 5; Sutinen and Middleton, 2021). When the SIS extended its margin to any of these moraine complexes, it would almost certainly cover the Parkajoki area (Fig. 5). Pinpointing the timing of formation of these moraines is therefore important to understand the ice-burial history of Parkajoki. Unfortunately, it remains unclear whether these moraines represent maximum extents of the ice sheet, or outline re-advance positions during overall retreat from one or several stadial maxima (Sutinen and Middleton, 2021). The southernmost of the moraine complexes near Pudasjärvi (Fig. 5) could represent an Early Weichselian maximum position of the ice sheet because it marks the location where a presumed Early Weichselian till bed tapers out towards the south (Johansson et al., 2011). Since an ice-sheet with its margin at the Pudasjärvi moraine could deposit the MIS 5b till bed recorded at Sokli, it seems likely that the Pudasjärvi End Moraine represents the maximum MIS 5b extent although it could also date from the retreat phase at the end MIS 4 (Sarala, 2005). Moraine complexes further north have also tentatively been correlated with MIS 5b. Although the northernmost of these moraines, the Porttipahta End Moraine (Fig. 5), has been dated to MIS 5d (Sutinen and Middleton, 2021), its age determination may have suffered from incomplete bleaching of the glaciofluvial sand as suggested for many other OSL sites in the region (e.g., Salonen et al., 2014; Lunkka et al., 2015; Åberg et al., 2020; Alexanderson et al., 2022). However, it is possible that the SIS covered the

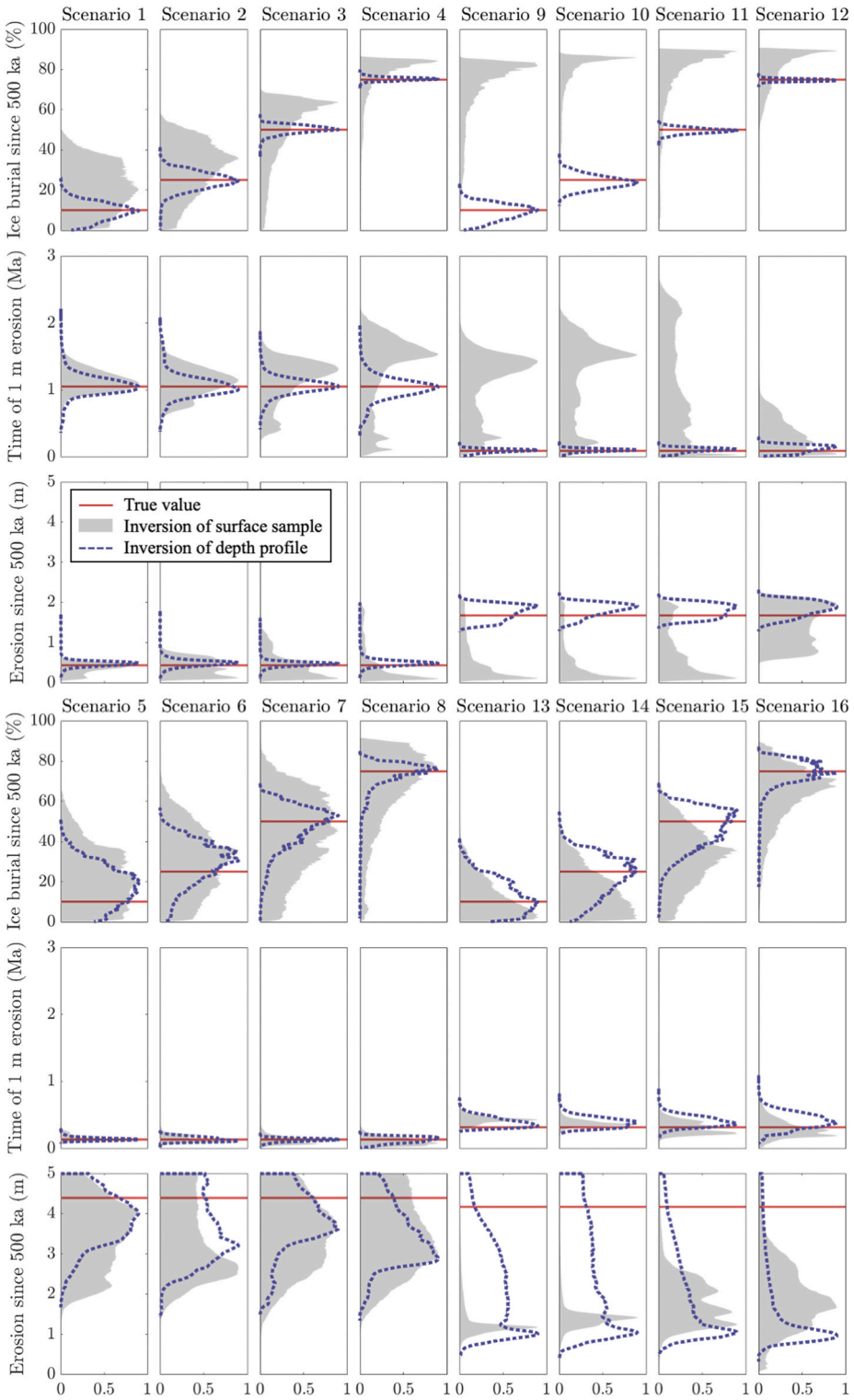


Fig. 4. Overview of the sixteen synthetic scenarios showing the derived parameters 'Ice burial since 500 ka (%)', 'Time of 1 m erosion (Ma)', and 'Erosion since 500 ka' with true values (red lines), and distribution of parameters for all accepted models from inversion of i) a surface sample alone (grey patch) and ii) a depth profile of 6 depth points down to 2 m depth (blue dashed curve). Scenarios 1–4 have a slow and steady exhumation since 2 Ma (Fig. 3a) whereas scenarios 9–12 have similarly slow total erosion rates, but experience episodic erosion of ~1.6 m thickness between ~135 and 15 ka (Fig. 3b). Scenarios 5–8 have relatively fast and steady exhumation since 2 Ma (Fig. 3c) whereas scenarios 13–16 have similar total erosion but experience decreasing erosion after 260 ka (Fig. 3d).

Parkajoki area during both MIS 5b and 5d. Because of the short distance between the Porttipahta End Moraine and Parkajoki (Fig. 5), we estimate that the MIS 5d ice burial was of shorter duration than during MIS 5b. A smaller MIS 5d extent of shorter duration is in line with the record from Sokli, the global ice volume record, and low inputs of IRD in the Arctic Ocean similar to Holocene values throughout the Eemian until 90 ka (MIS 5e-5c) followed by a marked increase between 90 and 80 ka (MIS 5b; Spielhagen et al., 2004; Svendsen et al., 2004). In our simple scenario, we therefore estimate full exposure of our sample sites for a minimum of 6 kyr (74–80 ka) and a maximum of 14 kyr (72–86 ka)

during the MIS 5a interstadial and a minimum of 12 kyr (93–105 ka) and a maximum of 16 kyr (92–108 ka) during the MIS 5c interstadial (Fig. 9a). However, we acknowledge that these values are not particularly well constrained.

3.4.1.4. Eemian exposure. Finally, we infer that Parkajoki was exposed during the Eemian (MIS 5e) period for a minimum of 10 ka between 130 and 120 ka to a maximum of 20 ka between 130 and 110 ka (Fig. 9a). This agrees with inferred Eemian-age deposits from Leveäniemi in northern Sweden (Fig. 6; Robertsson, 1997) and interglacial sediments dated to ~120–130 ka at Sokli in Finland (Fig. 5; Helmens et al., 2000; Alexanderson et al., 2008).

3.4.2. Pre-Eemian accumulation of cosmogenic ^{10}Be and ^{26}Al in Parkajoki tors

Based on the inferred minimum and maximum exposure estimates for the Holocene, Weichselian, and Eemian periods we calculate the resulting ^{10}Be and ^{26}Al inventories and ^{26}Al/^{10}Be ratio assuming no erosion (Fig. 9b–d). The results show that the measured cosmogenic nuclide inventories in the Naakakarhakka tor (barely) fit the maximum proposed exposure history down to ~60 cm depth for both ^{10}Be and ^{26}Al, whereas deeper samples exceed the maximum modelled concentrations. For the Lamuvaara tor, intermediate exposure scenarios are sufficient to fit the maximum proposed exposure history down to ~135 cm depth for both ^{10}Be and ^{26}Al, whereas deeper samples slightly exceed the maximum modelled concentrations. This demonstrates that both Parkajoki tors contain components of cosmogenic nuclides produced prior to the penultimate glacial maximum. We note that this simple analysis does not account for post-Saalian erosion, which would act to further increase the mismatch between measured and modelled concentrations.

4. Discussion

To end this paper, we summarize and contrast the significance of our results in the context of three topics: 1) the usefulness of cosmogenic depth profiles to constrain long-term erosion and exposure histories, 2) the ice-burial and erosion histories in Parkajoki and northeast Fennoscandia, and 3) the near-surface residence times of the Parkajoki tors and their constraints on the long-term landscape evolution.

4.1. Evaluating the usefulness of cosmogenic depth profiles to constrain long-term erosion and exposure histories

Cosmogenic depth profiles are commonly used to date sedimentary deposits such as fluvial terraces (e.g., Braucher et al., 2009; Hidy et al., 2010), periglacial and till deposits (e.g., Andersen et al., 2018), sub-ice sediments (Christ et al., 2021, 2023), or in-situ regolith (Ackerer et al., 2022), whereas examples of cosmogenic depth profiles in bedrock are less common but have seen a growing number of applications in recent years. Indeed, several recent studies present cosmogenic depth profiles in bedrock exposed at the surface today (Balter-Kennedy et al., 2021; Sugden et al., 2017) or currently buried by ice (Schaefer et al., 2016; Balco et al., 2023). In addition, several studies present pseudo-depth profiles by measuring cosmogenic nuclides in vertical profiles along tor slopes (Phillips et al., 2006; Raab et al., 2021; Máčka et al., 2023) or on differentially plucked/weathered tor surfaces (Margreth et al., 2016). Since measuring cosmogenic nuclides in a depth profile comes with additional project costs, often at the expense of analysing extra surface samples, a thorough evaluation of the added information that can be gained from depth profiles is important in order to determine their value. Inverse modelling of a range of synthetic scenarios is a powerful approach to discern which scenarios can be better resolved with cosmogenic depth profiles. The synthetic analyses presented in this study show that adding cosmogenic nuclide measurements at depths of

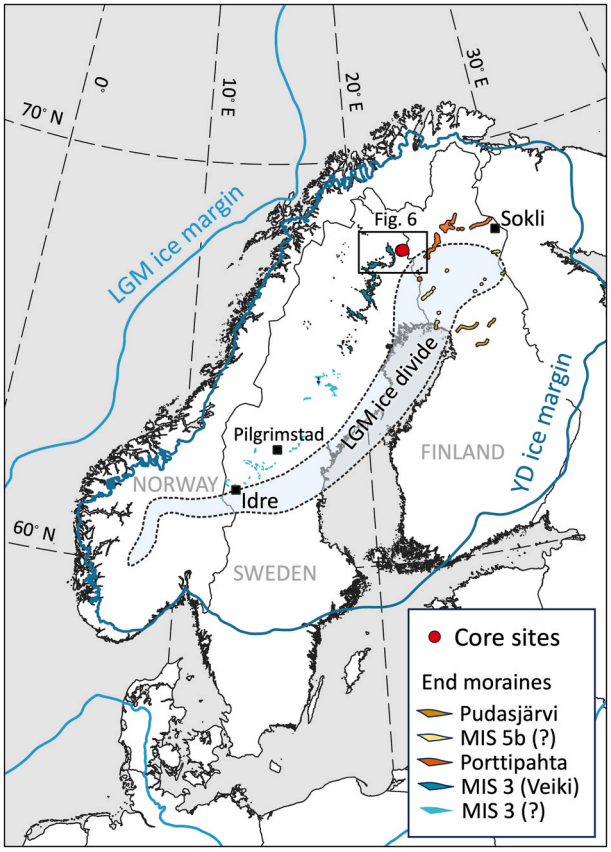


Fig. 5. Overview of the study area in Scandinavia and locations mentioned in text. LGM (Last Glacial Maximum, 21 ka) and YD (Younger Dryas, 12 ka) ice-sheet extent outlines ('max' extents from Hughes et al. (2016)). LGM ice divide from (Olsen et al., 2013). Finnish moraine sequences from Sutinen and Middleton (2021): Pudasjärvi (possibly MIS 5b), MIS 5b (? = uncertain), Porttipahta End Moraine (possibly MIS 5d), and Veiki (MIS 3) moraine extent from Peterson Becher et al. (2022), MIS 3 (?) marks dead-ice depressions hypothesized to be of same age as the Veiki moraine (Peterson Becher et al., 2022). The box outlines the Parkajoki area in northeastern Fennoscandia (Fig. 6).

up to ~2 m can provide additional information on ice-burial and erosion histories compared to a surface sample, especially when erosion rates are low, and cosmogenic nuclide concentrations are high. Indeed, our results show that inversion of a depth profile provides tight constraints on both erosion depths and ice-burial duration, even when inversion of a surface sample alone is unable to discern between long-term near-surface residence below bedrock and lengthy ice burial (Figs. 3–4). Our application of the method in the Parkajoki area of northeastern Sweden additionally shows that i) the depth profile approach is less sensitive to variations in ^{26}Al/^{10}Be ratios due to analytical errors (statistical outliers) than a single surface sample, and ii) extra information can be gained from a joined inversion of depth profiles from multiple sites with a common ice-burial history (Fig. 8). Furthermore, previous work has shown that the derived ice-burial history is insensitive to the details of the chosen climate curve (Andersen et al., 2023). Therefore the inverse-modelled ice-burial durations do not rely on a constant relation between ice burial and benthic marine δ^{18}O values over hundred-thousands to millions of years, as the integrated ice-burial duration parameter is not sensitive to the exact timing of ice-free periods. However, our results also demonstrate that relatively little extra information can be gained from measuring a depth profile if erosion rates are high and nuclide concentrations low (Fig. 3c and d; 4 scenario 5–8 and 13–16). For the future, targeting high polar and/or arid regions with very low erosion rates would probably lead to better constrained

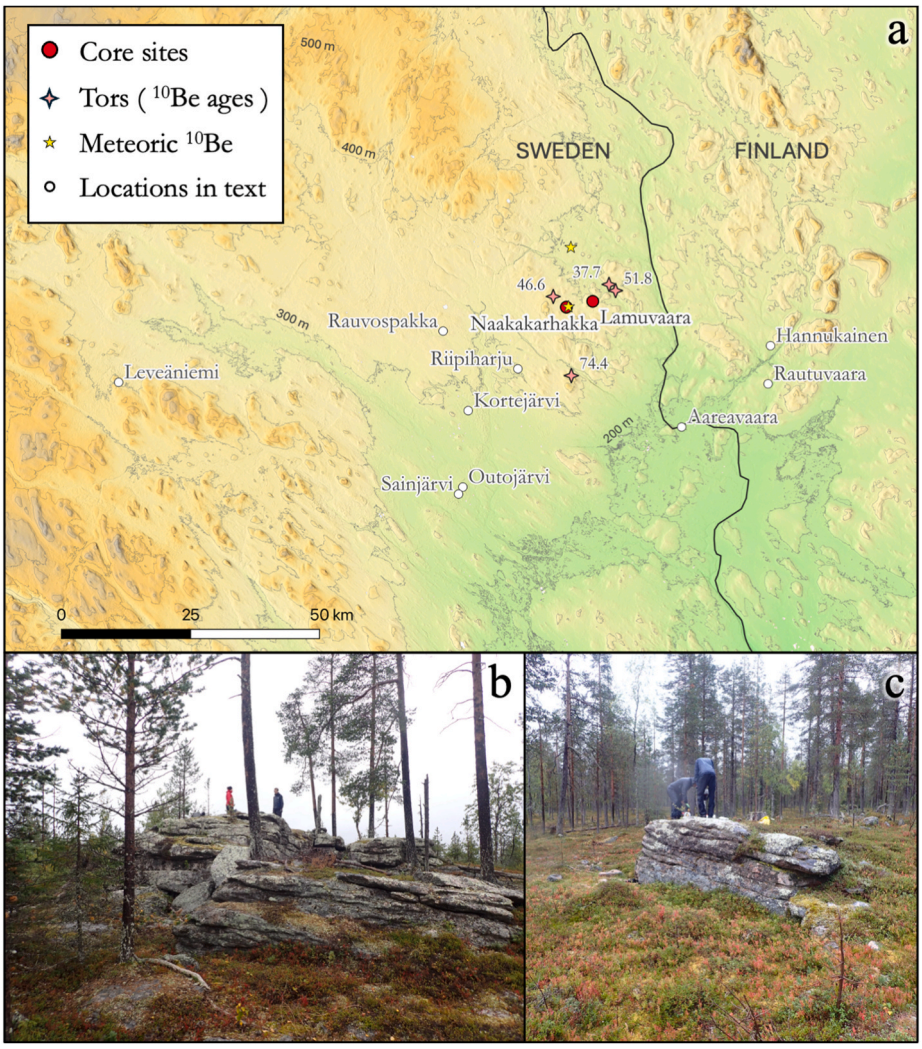


Fig. 6. a. Map of Parkajoki with locations of the Naakakarhakka and Lamuvaara core sites, published cosmogenic samples from other nearby tors (ages in kyr; Stroeven et al., 2006), meteoric ^{10}Be sites (Ebert et al., 2012), and other localities mentioned in text. The topography (colorscale and hillshade) and contours are from ArcticDEM (PGC; Porter et al., 2023), the contour interval is 100 m. Bedrock coring sites at b. Naakakarhakka and c. Lamuvaara. Surface samples from both sites were previously presented by Stroeven et al. (2002).

model parameters. Furthermore, improved quantification of production rates at depth would help narrow uncertainties on e.g. attenuation length scales and muon production parameters, which have an impact on long-term accumulation of cosmogenic nuclides (Balco, 2017). As an example, we investigate the sensitivity of our inversion results to the uncertainty related to the muon-production parametrization (<10% for high-latitude regions; Model 1A; Balco, 2017). Our results show that assuming a 5–10% too high or too low muon production lead to similar exhumation pathways, but a small offset in the distributions of the 'Ice burial since 500 ka' parameter compared to the true values (Supp. Fig. S6). This offset is on the order of 5–10 %.

We have shown that a cosmogenic depth profile adds information over a surface sample for the specific design of our forward model, but this is likely to be a robust find also if alternative or additional model parameters are considered. We note that the flexible design of our modelling setup allows for easy modification or replacement of the forward model while maintaining the inversion procedure. Some minor modifications to the forward model could enable the inclusion of other model parameters (such as periodic thin ice or snow cover), and by replacing the forward model the inversion code could be applied to constrain exposure and erosion histories in entirely different (e.g. non-glacial) settings.

4.2. Ice-burial duration and erosion at Parkajoki

Our estimated ice-burial duration of the Parkajoki area derived from cosmogenic nuclide depth profiles in two tors (~20–35% of the last 500 ka) overlaps the lower end of the estimated duration of Weichselian ice burial based on dating of scattered glacial records across north-eastern Fennoscandia (Section 3.4.1; Fig. 9) which corresponds to ice burial for 33–55 % of time since the end of the Eemian at 110 ka. However, both these estimates imply much less ice burial compared to previous estimates based on cosmogenic ^{10}Be and ^{26}Al in surface samples of the Parkajoki tors that suggested ice burial for 77% of time since 335 ka or 73% of time since 605 ka (Section 3.1; Stroeven et al., 2002), and a mean of 79% of time since 399 ka (Li et al., 2008). Likewise, the minimum estimates of tor erosion derived in this study (>1.7–2.2 m erosion since 500 ka, with the last 1 m of erosion being removed since ~0.1–0.3 Ma) is incompatible with a previous maximum erosion estimate based on cosmogenic surface concentrations (<1.6 m Myr^{-1}; Stroeven et al., 2002), with our minimum estimate exceeding the previous maximum estimate by more than a factor 2 when corrected for the different time scales. These discrepancies in ice-burial and erosion estimates are mutually dependent and result from a combination of two factors: First, the reported ^{26}Al/^{10}Be ratios in surface samples in Stroeven et al. (2002)

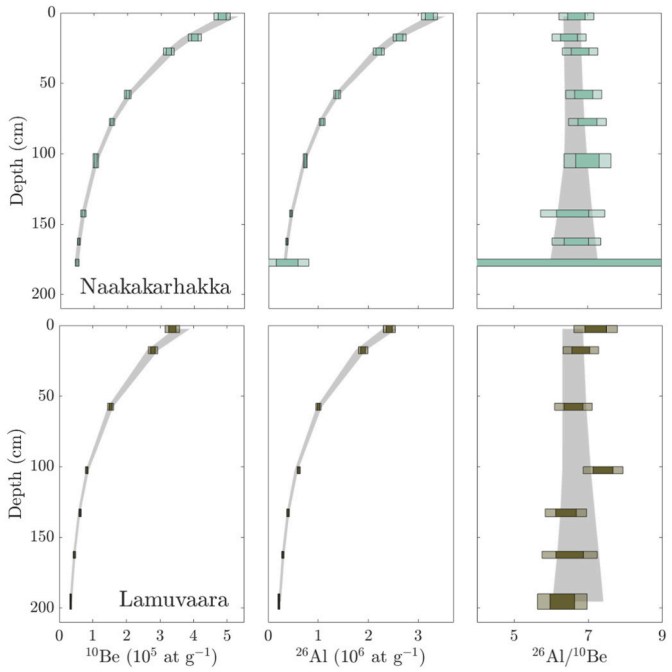


Fig. 7. Depth profiles of ^{10}Be, ^{26}Al, and ^{26}Al/^{10}Be from Naakakarhakka (top row) and Lamuvaara (bottom row) with boxes indicating 1σ and 2σ analytical uncertainty (x-direction) and thickness of sample (y-direction). Note that the ^{26}Al concentration of the lowest sample at Naakakarhakka has poor analytical resolution (Supp. Table S4) resulting in large errors on the ^{26}Al/^{10}Be ratio. Concentrations of accepted models from individual depth profile inversions are indicated with grey patches.

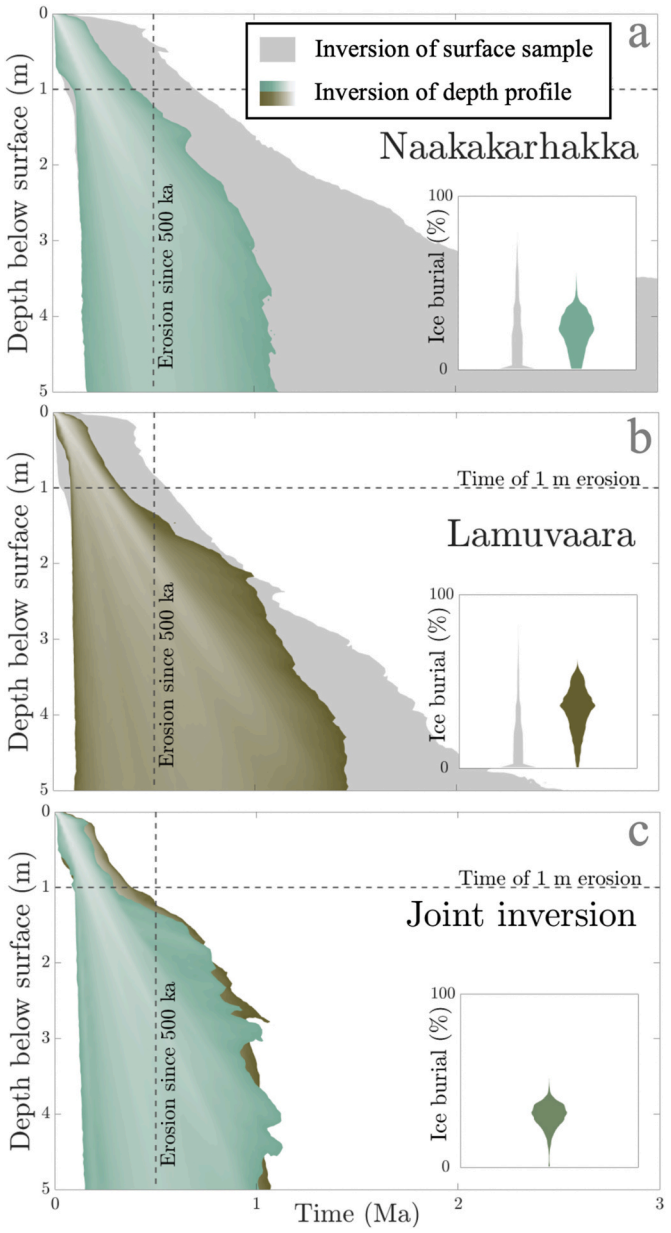


Fig. 8. Inversions of ^{10}Be and ^{26}Al data from a) Naakakarhakka, b) Lamuvaara, and c) joint for both sites. The main panels show depth profile inversion (green patches with light colors indicating a higher frequency of accepted models). Insets show the distribution of the derived parameter 'Ice burial since 500 ka (%)' for all accepted models for the depth profile inversion (green patches). In (a) and (b) the surface sample inversions are shown for comparison (grey patches in main panels and insets).

are lower (5.1–5.3 in original paper; 5.9–6.3 when an updated production ratio is used in Stroeven et al. (2016) supplement) than what we have obtained in this study (6.7–7.2 in the two surface samples; 6.8 ± 0.3 mean of all analyses). That we obtain higher ^{26}Al/^{10}Be ratios in surface samples collected adjacent to the original samples (and also in samples at depth) is probably an effect of improved techniques of analysing ^{26}Al and ^{10}Be in the 20+ years that have passed since the analyses for the Stroeven et al. (2002) paper were performed. Our analysis of CoQtz-N intercomparison material (Binnie et al., 2019) along with samples presented in this study gives us confidence in the precision and accuracy of the ^{10}Be and ^{26}Al analyses (Supp. Table S6; Supp. Fig. S5). Additionally, analyses of multiple samples in depth profiles allows us, through the inversion procedure, to average out random variations in ratios due to measurement uncertainties of each nuclide (Fig. 7). Second, the three models used for estimating erosion and exposure in Stroeven et al. (2002) either consider erosion and ice burial separately and therefore ignore their combined effect on nuclide concentrations and ratios. Or alternatively, for one model they include partial shielding by overlying mass (e.g., from regolith, till, or snow) during ice-free periods, but the ice-free periods are limited to occur when $\delta^{18}O \leq 3.7$ ‰ on the DSDP 607 marine benthic foraminifer oxygen isotope record (Raymo et al., 1989; Ruddiman et al., 1989; Lazarus et al., 1995), leading to a very high degree of ice burial. Li et al. (2008) allow the $\delta^{18}O$ threshold to vary between scenarios but apply steady erosion rates for ice-free and ice-covered conditions, which disregards the potential for episodic erosion. The lower ^{26}Al/^{10}Be ratios in the earlier studies combined with less encompassing modelling approaches lead to higher estimates of ice burial duration because the lower ratios are interpreted to be a result of excess ^{26}Al decay during ice burial (due to its shorter half-life than ^{10}Be). However, our analyses yielding updated ^{26}Al/^{10}Be ratios show these to be higher (and closer to the surface production ratio of ~6.75–7.3; Balco and Shuster, 2009; Corbett et al., 2017; Halsted et al., 2021) and our inverse model that consider a more complete spectrum of erosion and ice-burial scenarios leads us to update estimates of ice burial duration and erosion rates, arriving at a shorter duration of ice burial and a higher rate of erosion of the Parkajoki tors.

4.3. *Implications for landscape evolution in Parkajoki area*

Although our *minimum* erosion estimates from the Parkajoki tors more than double the previous *maximum* estimates, our maximum erosion rates on timescales of 500 ka are not as well constrained due to the inherent limitations of the cosmogenic method to resolve erosion beyond a few meters owing to the relatively shallow attenuation lengths of cosmogenic production. The current lack of a chronometer to record slow erosion on depth scales of a few tens to hundreds of meters over the

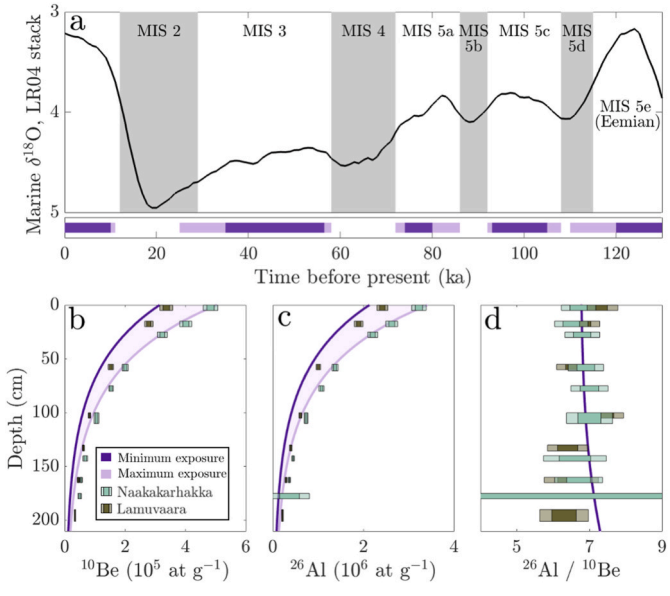


Fig. 9. Test of simple scenario: removal of all cosmogenic nuclides produced prior to the Saalian glaciation by glacial erosion during the penultimate glacial maximum. a) Marine Isotope Stages (MIS) and marine benthic d18O values in the LR04 stack (Lisiecki and Raymo, 2005) during the Eemian and Weichselian. The bars at the bottom indicate the timing and duration of ice-free periods during the Eemian and Weichselian for the maximum (light purple) and minimum (dark purple) end-member exposure histories inferred from nearby sites and regional reconstructions (see Sec. 3.4.1). b) ^{10}Be, and c) ^{26}Al, and d) ^{26}Al/^{10}Be depth profiles arising from maximum (light purple) and minimum (dark purple) exposure histories with semi-transparent red patch highlighting intermediate exposure, compared to measured nuclide inventories in Naakakarhakka and Lamuvaara tors.

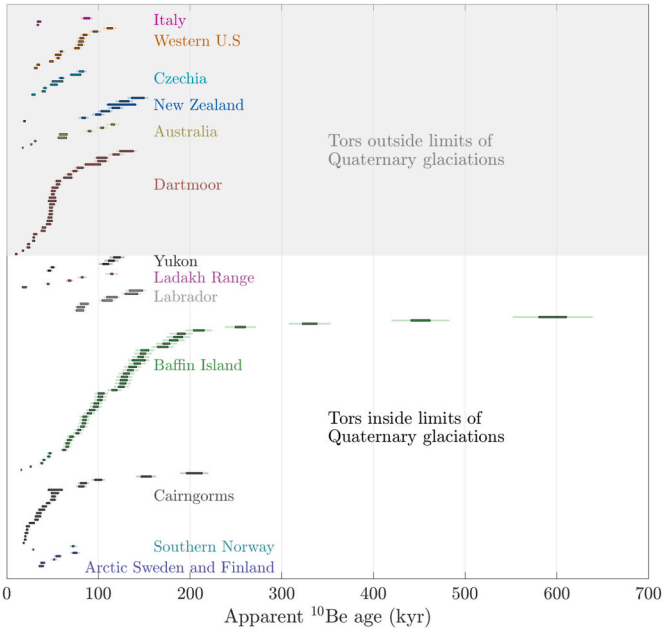


Fig. 10. Tor apparent ^{10}Be exposure ages outside and inside limits of Quaternary glaciations (see Supp. Table S7). Tors from Italy (Raab et al., 2018), Western U.S. (Small et al., 1997), Czechia (Máčka et al., 2023), New Zealand (Raab et al., 2021), Australia (Heimsath et al., 2001), Dartmoor (Gunnell et al., 2013), Ladakh Range in India (Dietsch et al., 2015), Yukon Territory (Stroeven et al., 2014), Labrador (Marquette et al., 2004), Baffin Island (Bierman et al., 1999; Briner et al., 2003, 2006; Margreth et al., 2016), Cairngorms (Phillips et al., 2006), Southern Norway (Andersen et al., 2018), Arctic Sweden (This study; Stroeven et al., 2006) and Finland (Darmody et al., 2008). Note that six of the Dartmoor tors (of median ages) were likely covered by a thin ice cap at the LGM (Evans et al., 2012; Gunnell et al., 2013). This compilation builds on and expands the compilation by Máčka et al. (2023). All ages are recalculated for direct comparison with new ages obtained in this study.

duration of the Quaternary inhibits quantifying the long-term efficiency of glacial erosion in the relatively low-relief landscape characteristic for northeast Fennoscandia including the Parkajoki area. However, we infer that the relatively high number of Weichselian sedimentary records in northeastern Fennoscandia compared to other regions indicates that glacial and non-glacial erosion during the Weichselian was relatively limited and sporadic in this region. In contrast, the lack of sedimentary records that unequivocally predate the Saalian glaciation indicate that erosion during the penultimate glacial maximum was perhaps more efficient than during the Weichselian. Parkajoki was located under a centre of ice-mass dispersal and/or divergent ice flow during the LGM and earlier glacial maxima in the Weichselian (Kleman et al., 1999; Kleman and Glasser, 2007). This may have contributed to the limited Weichselian erosion because ice-dispersal centres, despite high overburden pressures, tend to be associated with cold-based conditions due to advection of cold firn into the ice and because strain heating due to ice flow is minimized by the low ice-surface slope (Waller et al., 2012). Whereas convergent ice flow is generally associated with warm-based conditions and strong erosion (Kessler et al., 2008; Patton et al., 2022), divergent ice flow similarly leads to situations of weak erosion due to cold-based conditions (Patton et al., 2022). Cold-based ice generally inhibits erosion and acts to preserve landscapes (Kleman, 1994; Waller et al., 2012). However, the Late Saalian ice sheet was more extensive and lasted perhaps longer than those of the Weichselian (Svendsen et al., 2004; Batchelor et al., 2019). The more extensive (and likely thicker) Saalian ice sheet probably had a centre of mass dispersal east of the Parkajoki area (Colleoni et al., 2016), which could have resulted in more subglacial erosion. Furthermore, the thicker ice and longer duration of ice cover could be important in subglacial ice reaching the pressure melting point (Kleman et al., 1997; Cutler et al., 2000; Hättestrand and Stroeven, 2002; Waller et al., 2012) and thereby for the ice sheet to remove sedimentary archives and potentially erode into bedrock. However, it is important to note that our analysis of a simple erosion scenario where all cosmogenic nuclides were removed by erosion in the Saalian (Section 3.4) does not satisfactorily match our measured nuclide concentrations at depth (Fig. 9). If the cosmogenic nuclide production parameters (production rates and attenuation lengths for spallogenic and muon production pathways) are adequately constrained, this either means that Weichselian exposure duration was even longer than our reconstructed maximum scenario, or that some amount of nuclide inheritance remains from pre-Late Saalian exposure, perhaps formed by muon-production at rock depths of a few meters (Briner et al., 2016). That erosion at Parkajoki was relatively shallow even under a more extensive Late-Saalian ice sheet is in accordance with the lack of large streamlined bedrock landforms such as rock drumlins in the Parkajoki area which indicate limited glacial remoulding of bedrock landforms compared to neighbouring regions (Hättestrand and Stroeven, 2002; Hättestrand et al., 2004; Ebert et al., 2015). It is also in accordance with the meteoric ^{10}Be inventory in nearby saprolite suggesting saprolite residence times >0.8 Ma (Ebert et al., 2012).

The erosion rates derived in this study (>1.7–2.2 m erosion since 500 ka) entail substantial Quaternary modification of the Parkajoki tor landforms relative to their present relief of ~1–5 m above the ground surface (Fig. 6) while they continue at least 0.5 m below ground into the surrounding grus cover (Stroeven et al., 2002). The apparent ^{10}Be ages from the Parkajoki tors and other tors in Arctic Sweden (Stroeven et al., 2006) and Finland (Darmody et al., 2008), roughly correspond to apparent ages derived from tors in other parts of the world, both within and outside the limits of Quaternary glaciations (Fig. 10; Supp. Table S8). However, ages >100 kyr, found in other glaciated regions such as the Cairngorms (Phillips et al., 2006), Baffin Island (Bierman

et al., 1999; Briner et al., 2003, 2006; Margreth et al., 2016), Labrador (Marquette et al., 2004), Yukon Territory (Stroeven et al., 2014), and the Ladakh Range in India (Dietsch et al., 2015), have not yet been found within Fennoscandia, although this could be an effect of the relatively small number of dated tors.

5. Conclusions

In this study, we have investigated the application of shallow cosmogenic depth profiles in bedrock to constrain long-term ice-burial and erosion histories. Based on inverse modelling of a suite of synthetic scenarios, we conclude that depth-profile inversions yield a better fit to true exposure and exhumation histories than inversions from surface samples across all examined exhumation patterns. This is the case even in complex scenarios where rapid erosion follows prolonged slow erosion – situations that surface sample inversions struggle to constrain. However, the improvement is modest in some high-erosion scenarios, in part because the sensitivity to past ice-burial and erosion decreases when the inherited signal approaches the uncertainty. Indeed, depth-profile inversions resolve the true ice-sheet burial scenarios across a range of ice-burial durations (10%–75% ice burial since 500 ka), but the combination of short ice-burial durations and high erosion rates result in both wider ranges in parameter value and less accurate results.

Applying the depth-profile inversion method to two tors in the Parkajoki region of northeastern Sweden, we also find that the range of potential ice-burial histories narrows when compared to surface samples alone, but the ice-burial duration parameter remains relatively poorly resolved. When performing a joint inversion of both tors, the ice-burial duration is 12.8–40.7% of time since 500 ka. Comparing these results to synthetic scenarios with similar exhumation histories, we estimate that the true burial duration of the Parkajoki tors was most likely ~20–35% of time since 500 ka. The corresponding range in erosion depths yields ~2–10 m since 500 ka, but the high end of this estimate is more uncertain owing to the relatively shallow attenuation lengths of cosmogenic production.

Based on existing exposure estimates from northeastern Fennoscandia for the Holocene, Weichselian, and Eemian periods we show that the measured cosmogenic nuclide inventories in the Parkajoki tors contain some component of cosmogenic nuclides produced prior to the penultimate glacial maximum (Late Saalian).

Code availability

Spreadsheets and MATLAB code used for the MCMC inversions can be downloaded from https://github.com/jaluan/depth-profile-inversion.

Declaration of competing interest

The authors declare that they have no known competing financial interests or personal relationships that could have appeared to influence the work reported in this paper.

Acknowledgements

This work was supported by a research grant (15467) from the Villum Foundation. We thank Esben Palmstrøm for help in the field, and Birte Lindahl Eriksen and Rikke Brok Jensen for help with processing the samples in the laboratory. We thank Derek Fabel and Clas Hättestrand for checking their old field notes and data. We appreciate the reviews by Keir Nichols and Ángel Rodés that helped improve the manuscript.

Appendix A. Supplementary data

Supplementary data to this article can be found online at https://doi.org/10.1016/j.quascirev.2024.109010.

Data availability

All data are included in the manuscript and supplementary information.

References

Åberg, A.K., Kultti, S., Kaakinen, A., Eskola, K.O., Salonen, V.-P., 2020. Weichselian sedimentary record and ice-flow patterns in the Sodankylä area, central Finnish Lapland. Bull. Geol. Soc. Finland 92 (2), 77–98. https://doi.org/10.17741/bgsf/92.2.001.

Ackerer, J., Van der Woerd, J., Meriaux, A.S., Ranchoux, C., Schäfer, G., Delay, F., Chabaux, F., 2022. Quantifying geomorphological evolution from 10Be denudation rates: insights from high-resolution depth profiles, topsoils, and stream sediments (Strengbach CZO, France). Earth Surf. Process. Landforms 47 (14), 3239–3258. https://doi.org/10.1002/esp.5454.

Alexanderson, H., Eskola, K.O., Helmens, K.F., 2008. Optical dating of a late Quaternary sediment sequence from Sokli, northern Finland. Geochronometria 32 (1), 51–59. https://doi.org/10.2478/v10003-008-0022-9.

Alexanderson, H., Hättestrand, M., Lindqvist, M.A., Sigfúsdóttir, T., 2022. MIS 3 age of the Veiki moraine in N Sweden – dating the landform record of an intermediate-sized ice sheet in Scandinavia. Arctic Antarct. Alpine Res. 54 (1), 239–261. https://doi.org/10.1080/15230430.2022.2091308.

Alexanderson, H., Johnsen, T., Murray, A.S., 2010. Re-dating the Pilgrimstad Interstadial with OSL: a warmer climate and a smaller ice sheet during the Swedish Middle Weichselian (MIS 3)? Boreas 39 (2), 367–376. https://doi.org/10.1111/j.1502-3885.2009.00130.x.

Andersen, J.L., Egholm, D.L., Knudsen, M.F., Linge, H., Jansen, J.D., Goodfellow, B.W., Pedersen, V.K., Tikhomirov, D., Olsen, J., Fredin, O., 2018. Pleistocene evolution of a Scandinavian plateau landscape. J. Geophys. Res.: Earth Surf. 123 (12), 3370–3387. https://doi.org/10.1029/2018JF004670.

Andersen, J.L., Egholm, D.L., Olsen, J., Larsen, N.K., Knudsen, M.F., 2020. Topographical evolution and glaciation history of South Greenland constrained by paired 26Al/10Be nuclides. Earth Planet Sci. Lett. 542, 116300. https://doi.org/10.1016/j.epsl.2020.116300.

Andersen, J.L., Newall, J.C., Fredin, O., Glasser, N.F., Lifton, N.A., Stuart, F.M., Fabel, D., Caffee, M., Pedersen, V.K., Koester, A.J., Suganuma, Y., Harbor, J.M., Stroeven, A.P., 2023. A topographic hinge-zone divides coastal and inland ice dynamic regimes in East Antarctica. Communications Earth & Environment 4 (1). https://doi.org/10.1038/s43247-022-00673-6.

Balco, G., 2017. Production rate calculations for cosmic-ray-muon-produced 10Be and 26Al benchmarked against geological calibration data. Quat. Geochronol. 39, 150–173. https://doi.org/10.1016/j.quageo.2017.02.001.

Balco, G., Brown, N., Nichols, K., Venturelli, R.A., Adams, J., Braddock, S., Campbell, S., Goehring, B., Johnson, J.S., Rood, D.H., Wilcken, K., Hall, B., Woodward, J., 2023. Reversible ice sheet thinning in the amundsen sea embayment during the late Holocene. Cryosphere 17 (4), 1787–1801. https://doi.org/10.5194/tc-17-1787-2023.

Balco, G., Shuster, D.L., 2009. 26Al–10Be–21Ne burial dating. Earth Planet Sci. Lett. 286 (3), 570–575. https://doi.org/10.1016/j.epsl.2009.07.025.

Balter-Kennedy, A., Young, N.E., Briner, J.P., Graham, B.L., Schaefer, J.M., 2021. Centennial- and orbital-scale erosion beneath the Greenland ice sheet near jakobshavn isbræ. J. Geophys. Res.: Earth Surf. 126 (12), e2021JF006429. https://doi.org/10.1029/2021JF006429.

Batchelor, C.L., Margold, M., Krapp, M., Murton, D.K., Dalton, A.S., Gibbard, P.L., Stokes, C.R., Murton, J.B., Manica, A., 2019. The configuration of Northern Hemisphere ice sheets through the Quaternary. Nat. Commun. 10 (1). https://doi.org/10.1038/s41467-019-11601-2. Article 1.

Bierman, P.R., Marsella, K.A., Patterson, C., Davis, P.T., Caffee, M., 1999. Mid-Pleistocene cosmogenic minimum-age limits for pre-Wisconsinan glacial surfaces in southwestern Minnesota and southern Baffin Island: a multiple nuclide approach. Geomorphology 27 (1), 25–39. https://doi.org/10.1016/S0169-555X(98)00088-9.

Binnie, S.A., Dewald, A., Heinze, S., Voronina, E., Hein, A., Wittmann, H., von Blanckenburg, F., Hetzel, R., Christl, M., Schaller, M., Léanni, L., Aster, Team, Hippe, K., Vockenhuber, C., Ivy-Ochs, S., Maden, C., Fülöp, R.-H., Fink, D., Wilcken, K.M., et al., 2019. Preliminary results of CoQtz-N: a quartz reference material for terrestrial in-situ cosmogenic 10Be and 26Al measurements. Nucl. Instrum. Methods Phys. Res. Sect. B Beam Interact. Mater. Atoms 456, 203–212. https://doi.org/10.1016/j.nimb.2019.04.073.

Borchers, B., Marrero, S., Balco, G., Caffee, M., Goehring, B., Lifton, N., Nishiizumi, K., Phillips, F., Schaefer, J., Stone, J., 2016. Geological calibration of spallation production rates in the CRONUS-Earth project. Quat. Geochronol. 31, 188–198. https://doi.org/10.1016/j.quageo.2015.01.009.

Braucher, R., Del Castillo, P., Siame, L., Hidy, A.J., Bourlés, D.L., 2009. Determination of both exposure time and denudation rate from an in situ-produced 10Be depth profile: a mathematical proof of uniqueness. Model sensitivity and applications to natural cases. Quat. Geochronol. 4 (1), 56–67. https://doi.org/10.1016/j.quageo.2008.06.001.

Briner, J.P., Goehring, B.M., Mangerud, J., Svendsen, J.I., 2016. The deep accumulation of 10Be at Utsira, southwestern Norway: implications for cosmogenic nuclide exposure dating in peripheral ice sheet landscapes. Geophys. Res. Lett. 43 (17), 9121–9129. https://doi.org/10.1002/2016GL070100.

Briner, J.P., Lifton, N.A., Miller, G.H., Refsnider, K., Anderson, R., Finkel, R., 2014. Using in situ cosmogenic 10Be, 14C, and 26Al to decipher the history of polythermal ice

sheets on Baffin Island, Arctic Canada. Quat. Geochronol. 19, 4–13. https://doi.org/10.1016/j.quageo.2012.11.005.
Briner, J.P., Miller, G.H., Davis, P.T., Bierman, P.R., Caffee, M., 2003. Last Glacial Maximum ice sheet dynamics in Arctic Canada inferred from young erratics perched on ancient tors. Quat. Sci. Rev. 22 (5), 437–444. https://doi.org/10.1016/S0277-3791(03)00003-9.
Briner, J.P., Miller, G.H., Davis, P.T., Finkel, R.C., 2006. Cosmogenic radionuclides from fiord landscapes support differential erosion by overriding ice sheets. GSA Bulletin 118 (3–4), 406–420. https://doi.org/10.1130/B25716.1.
Child, D., Elliott, G., Mifsud, C., Smith, A.M., Fink, D., 2000. Sample processing for earth science studies at ANTARES. Nucl. Instrum. Methods Phys. Res. Sect. B Beam Interact. Mater. Atoms 172 (1), 856–860. https://doi.org/10.1016/S0168-583X(00)00198-1.
Chmeleff, J., von Blanckenburg, F., Kossert, K., Jakob, D., 2010. Determination of the 10Be half-life by multicollector ICP-MS and liquid scintillation counting. Nucl. Instrum. Methods Phys. Res. Sect. B Beam Interact. Mater. Atoms 268 (2), 192–199. https://doi.org/10.1016/j.nimb.2009.09.012.
Christ, A.J., Bierman, P.R., Schaefer, J.M., Dahl-Jensen, D., Steffensen, J.P., Corbett, L.B., Peteet, D.M., Thomas, E.K., Steig, E.J., Rittenour, T.M., Tison, J.-L., Blard, P.-H., Perdrial, N., Dethier, D.P., Lini, A., Hidy, A.J., Caffee, M.W., Southon, J., 2021. A multimillion-year-old record of Greenland vegetation and glacial history preserved in sediment beneath 1.4 km of ice at Camp Century. Proc. Natl. Acad. Sci. USA 118 (13), e2021442118. https://doi.org/10.1073/pnas.2021442118.
Christ, A.J., Rittenour, T.M., Bierman, P.R., Keisling, B.A., Knutz, P.C., Thomsen, T.B., Keulen, N., Fosdick, J.C., Hemming, S.R., Tison, J.-L., Blard, P.-H., Steffensen, J.P., Caffee, M.W., Corbett, L.B., Dahl-Jensen, D., Dethier, D.P., Hidy, A.J., Perdrial, N., Peteet, D.M., et al., 2023. Deglaciation of northwestern Greenland during marine isotope stage 11. Science 381 (6655), 330–335. https://doi.org/10.1126/science.ade4248.
Colleoni, F., Wekerle, C., Näslund, J.-O., Brandefelt, J., Masina, S., 2016. Constraint on the penultimate glacial maximum Northern Hemisphere ice topography (≈140 kyrs BP). Quat. Sci. Rev. 137, 97–112. https://doi.org/10.1016/j.quascirev.2016.01.024.
Corbett, L.B., Bierman, P.R., Rood, D.H., Caffee, M.W., Lifton, N.A., Woodruff, T.E., 2017. Cosmogenic 26Al/10Be surface production ratio in Greenland. Geophys. Res. Lett. 44 (3), 1350–1359. https://doi.org/10.1002/2016GL071276.
Cutler, P.M., MacAyeal, D.R., Mickelson, D.M., Parizek, B.R., Colgan, P.M., 2000. A numerical investigation of ice-lobe–permafrost interaction around the southern Laurentide ice sheet. J. Glaciol. 46 (153), 311–325. https://doi.org/10.3189/172756500781832800.
Dalton, A.S., Stokes, C.R., Batchelor, C.L., 2022a. Evolution of the laurentide and innuitian ice sheets prior to the last glacial maximum (115 ka to 25 ka). Earth Sci. Rev. 224, 103875. https://doi.org/10.1016/j.earscirev.2021.103875.
Dalton, A.S., Pico, T., Gowan, E.J., Clague, J.J., Forman, S.L., McMartin, I., Sarala, P., Helmens, K.F., 2022b. The marine δ18O record overestimates continental ice volume during Marine Isotope Stage 3. Global Planet. Change 212, 103814. https://doi.org/10.1016/j.gloplacha.2022.103814.
Darmody, R.G., Thorn, C.E., Seppälä, M., Campbell, S.W., Li, Y.K., Harbor, J., 2008. Age and weathering status of granite tors in Arctic Finland (~68° N). Geomorphology 94 (1), 10–23. https://doi.org/10.1016/j.geomorph.2007.04.006.
Dietsch, C., Dortch, J.M., Reynhout, S.A., Owen, L.A., Caffee, M.W., 2015. Very slow erosion rates and landscape preservation across the southwestern slope of the Ladakh Range, India. Earth Surf. Process. Landforms 40 (3), 389–402. https://doi.org/10.1002/esp.3640.
Dunai, T.J., 2010. Cosmogenic Nuclides: Principles, Concepts and Applications in the Earth Surface Sciences. Cambridge University Press.
Ebert, K., Hall, A.M., Kleman, J., Andersson, J., 2015. Unequal ice-sheet erosional impacts across low-relief shield terrain in northern Fennoscandia. Geomorphology 233, 64–74. https://doi.org/10.1016/j.geomorph.2014.09.024.
Ebert, K., Willenbring, J., Norton, K.P., Hall, A., Hättestrand, C., 2012. Meteoric 10Be concentrations from saprolite and till in northern Sweden: implications for glacial erosion and age. Quat. Geochronol. 12, 11–22. https://doi.org/10.1016/j.quageo.2012.05.005.
Evans, D.J.A., Harrison, S., Vieli, A., Anderson, E., 2012. The glaciation of Dartmoor: the southernmost independent Pleistocene ice cap in the British Isles. Quat. Sci. Rev. 45, 31–53. https://doi.org/10.1016/j.quascirev.2012.04.019.
Farmer, J.R., Pico, T., Underwood, O.M., Cleveland Stout, R., Granger, J., Cronin, T.M., Fripiat, F., Martínez-García, A., Haug, G.H., Sigman, D.M., 2023. The bering strait was flooded 10,000 years before the last glacial maximum. Proc. Natl. Acad. Sci. USA 120 (1), e2206742119. https://doi.org/10.1073/pnas.2206742119.
Gunnell, Y., Jarman, D., Braucher, R., Calvet, M., Delmas, M., Leanni, L., Bourlès, D., Arnold, M., Aumaître, G., Keddaouche, K., 2013. The granite tors of Dartmoor, Southwest England: rapid and recent emergence revealed by Late Pleistocene cosmogenic apparent exposure ages. Quat. Sci. Rev. 61, 62–76. https://doi.org/10.1016/j.quascirev.2012.11.005.
Halsted, C.T., Bierman, P.R., Balco, G., 2021. Empirical evidence for latitude and altitude variation of the in situ cosmogenic 26Al/10Be production ratio. Geosciences 11 (10). https://doi.org/10.3390/geosciences11100402. Article 10.
Hättestrand, C., Götz, S., Näslund, J.-O., Fabel, D., Stroeven, A.P., 2004. Drumlin Formation time: evidence from northern and Central Sweden. Geogr. Ann. Phys. Geogr. 86 (2), 155–167. https://doi.org/10.1111/j.0435-3676.2004.00221.x.
Hättestrand, C., Stroeven, A.P., 2002. A relict landscape in the centre of Fennoscandian glaciation: geomorphological evidence of minimal Quaternary glacial erosion. Geomorphology 44 (1), 127–143. https://doi.org/10.1016/S0169-555X(01)00149-0.
Hättestrand, M., Robertsson, A.-M., 2010. Weichselian interstadials at Riipiharju, northern Sweden – interpretation of vegetation and climate from fossil and modern pollen records. Boreas 39 (2), 296–311. https://doi.org/10.1111/j.1502-3885.2009.00129.x.
Heimsath, A.M., Chappell, J., Dietrich, W.E., Nishiizumi, K., Finkel, R.C., 2001. Late Quaternary erosion in southeastern Australia: a field example using cosmogenic nuclides. Quat. Int. 83–85, 169–185. https://doi.org/10.1016/S1040-6182(01)00038-6.
Helmens, K.F., 2014. The Last Interglacial–Glacial cycle (MIS 5–2) re-examined based on long proxy records from central and northern Europe. Quat. Sci. Rev. 86, 115–143. https://doi.org/10.1016/j.quascirev.2013.12.012.
Helmens, K.F., Räsänen, M.E., Johansson, P.W., Jungner, H., Korjonen, K., 2000. The last interglacial-glacial cycle in ne Fennoscandia: a nearly continuous record from Sokli (Finnish lapland). Quat. Sci. Rev. 19 (16), 1605–1623. https://doi.org/10.1016/S0277-3791(00)00004-4.
Helmens, K.F., Risberg, J., Jansson, K.N., Weckström, J., Berntsson, A., Tillman, P.K., Johansson, P.W., Wastegård, S., 2009. Early MIS 3 glacial lake evolution, ice-marginal retreat pattern and climate at Sokli (northeastern Fennoscandia). Quat. Sci. Rev. 28 (19), 1880–1894. https://doi.org/10.1016/j.quascirev.2009.03.001.
Hidy, A.J., Gosse, J.C., Pederson, J.L., Mattern, J.P., Finkel, R.C., 2010. A geologically constrained Monte Carlo approach to modeling exposure ages from profiles of cosmogenic nuclides: an example from Lees Ferry, Arizona. G-cubed 11 (9). https://doi.org/10.1029/2010GC003084.
Hirvas, H., 1995. Glacial stratigraphy of northern Finland. In: Glacial Deposits in Northeast Europe. CRC Press.
Hughes, A.L.C., Gyllencreutz, R., Lohne, Ø.S., Mangerud, J., Svendsen, J.I., 2016. The last Eurasian ice sheets – a chronological database and time-slice reconstruction, DATED-1. Boreas 45 (1), 1–45. https://doi.org/10.1111/bor.12142.
Jansen, J.D., Knudsen, M.F., Andersen, J.L., Heyman, J., Egholm, D.L., 2019. Erosion rates in Fennoscandia during the past million years. Quat. Sci. Rev. 207, 37–48. https://doi.org/10.1016/j.quascirev.2019.01.010.
Johansson, P., Lunkka, J.P., Sarala, P., 2011. Chapter 9—the glaciation of Finland. In: Ehlers, J., Gibbard, P.L., Hughes, P.D. (Eds.), Developments in Quaternary Sciences. Elsevier, pp. 105–116. https://doi.org/10.1016/B978-0-444-53447-7.00009-X.
Kessler, M.A., Anderson, R.S., Briner, J.P., 2008. Fjord insertion into continental margins driven by topographic steering of ice. Nat. Geosci. 1 (6), 365–369. https://doi.org/10.1038/ngeo201.
Kleman, J., 1992. The Palimpsest Glacial Landscape in Northwestern Sweden: late Weichselian deglaciation landforms and traces of older west-centered ice sheets. Geogr. Ann. Phys. Geogr. 74 (4), 305–325. https://doi.org/10.1080/04353676.1992.11880373.
Kleman, J., 1994. Preservation of landforms under ice sheets and ice caps. Geomorphology 9 (1), 19–32. https://doi.org/10.1016/0169-555X(94)90028-0.
Kleman, J., Glasser, N.F., 2007. The subglacial thermal organisation (STO) of ice sheets. Quat. Sci. Rev. 26 (5), 585–597. https://doi.org/10.1016/j.quascirev.2006.12.010.
Kleman, J., Hättestrand, C., Borgström, I., Stroeven, A., 1997. Fennoscandian palaeoglaciology reconstructed using a glacial geological inversion model. J. Glaciol. 43 (144), 283–299. https://doi.org/10.3189/S0022143000003233.
Kleman, J., Hättestrand, C., Clarhäll, A., 1999. Zooming in on frozen-bed patches: scale-dependent controls on Fennoscandian ice sheet basal thermal zonation. Ann. Glaciol. 28, 189–194. https://doi.org/10.3189/172756499781821670.
Kleman, J., Hättestrand, M., Borgström, I., Fabel, D., Preusser., F., 2021. Age and duration of a MIS 3 interstadial in Fennoscandian Ice Sheet core area - implications for ice sheet dynamics. Quat. Sci. Rev. 264, 107011.
Kleman, J., Hättestrand, M., Borgström, I., Preusser, F., Fabel, D., 2020. The Idre marginal moraine – an anchorpoint for Middle and Late Weichselian ice sheet chronology. Quaternary Science Advances 2, 100010. https://doi.org/10.1016/j.qsa.2020.100010.
Knudsen, M.F., Egholm, D.L., 2018. Constraining Quaternary ice covers and erosion rates using cosmogenic 26Al/10Be nuclide concentrations. Quat. Sci. Rev. 181, 65–75. https://doi.org/10.1016/j.quascirev.2017.12.012.
Knudsen, M.F., Egholm, D.L., Jacobsen, B.H., Larsen, N.K., Jansen, J.D., Andersen, J.L., Linge, H.C., 2015. A multi-nuclide approach to constrain landscape evolution and past erosion rates in previously glaciated terrains. Quat. Geochronol. 30, 100–113. https://doi.org/10.1016/j.quageo.2015.08.004.
Kohl, C.P., Nishiizumi, K., 1992. Chemical isolation of quartz for measurement of in-situ -produced cosmogenic nuclides. Geochem. Cosmochim. Acta 56 (9), 3583–3587. https://doi.org/10.1016/0016-7037(92)90401-4.
Korschinek, G., Bergmaier, A., Faestermann, T., Gerstmann, U.C., Knie, K., Rugel, G., Wallner, A., Dillmann, I., Dollinger, G., von Gostomski, Ch L., Kossert, K., Maiti, M., Poutivtsev, M., Remmert, A., 2010. A new value for the half-life of 10Be by Heavy-Ion Elastic Recoil Detection and liquid scintillation counting. Nucl. Instrum. Methods Phys. Res. Sect. B Beam Interact. Mater. Atoms 268 (2), 187–191. https://doi.org/10.1016/j.nimb.2009.09.020.
Lazarus, D., Spencer-Cervato, C., Pika-Biolzi, M., Beckmann, J.P., von Salis, K., Hilbrecht, H., Thierstein, H., 1995. Revised chronology of neogene DSDP holes from the world ocean. Ocean Drill. Prog. Tech. Rep. 24.
Li, Y., Fabel, D., Stroeven, A.P., Harbor, J., 2008. Unraveling complex exposure-burial histories of bedrock surfaces under ice sheets by integrating cosmogenic nuclide concentrations with climate proxy records. Geomorphology 99 (1), 139–149. https://doi.org/10.1016/j.geomorph.2007.10.010.
Lifton, N., Sato, T., Dunai, T.J., 2014. Scaling in situ cosmogenic nuclide production rates using analytical approximations to atmospheric cosmic-ray fluxes. Earth Planet Sci. Lett. 386, 149–160. https://doi.org/10.1016/j.epsl.2013.10.052.
Lisiecki, L.E., Raymo, M.E., 2005. A Pliocene-Pleistocene stack of 57 globally distributed benthic δ18O records. Paleoceanography 20 (1). https://doi.org/10.1029/2004PA001071.

Lunkka, J.P., Sarala, P., Gibbard, P.L., 2015. The Rautuvaara section, western Finnish Lapland, revisited – new age constraints indicate a complex Scandinavian Ice Sheet history in northern Fennoscandia during the Weichselian Stage. Boreas 44 (1), 68–80. https://doi.org/10.1111/bor.12088.

Máčka, Z., Braucher, R., Migoń, P., Belova, O., Leichmann, J., Aumaître, G., Bourlès, D., Keddadouche, K., 2023. Gneissic tors in the central European upland: complex Late Pleistocene forms? Geomorphology 436, 108764. https://doi.org/10.1016/j.geomorph.2023.108764.

Mäkinen, K., 2005. Dating the weichselian deposits of southwestern Finnish lapland. Quaternary studies in the northern and Arctic regions of Finland 40, 67–78.

Mangerud, J., 2004. Ice sheet limits on Norway and the Norwegian continental shelf. Quaternary Glaciations—Extent and Chronology 1, 271–294.

Mangerud, J., Alexanderson, H., Birks, H.H., Paus, A., Perić, Z.M., Svendsen, J.I., 2023. Did the Eurasian ice sheets melt completely in early Marine Isotope Stage 3? New evidence from Norway and a synthesis for Eurasia. Quat. Sci. Rev. 311, 108136. https://doi.org/10.1016/j.quascirev.2023.108136.

Mangerud, J., Gyllencreutz, R., Lohne, Ø., Svendsen, J.I., 2011. Chapter 22—glacial history of Norway. In: Ehlers, J., Gibbard, P.L., Hughes, P.D. (Eds.), Developments in Quaternary Sciences. Elsevier, pp. 279–298. https://doi.org/10.1016/B978-0-444-53447-7.00022-2.

Margreth, A., Gosse, J.C., Dyke, A.S., 2016. Quantification of subaerial and episodic subglacial erosion rates on high latitude upland plateaus: cumberland Peninsula, Baffin Island, Arctic Canada. Quat. Sci. Rev. 133, 108–129. https://doi.org/10.1016/j.quascirev.2015.12.017.

Marquette, G.C., Gray, J.T., Gosse, J.C., Courchesne, F., Stockli, L., Macpherson, G., Finkel, R., 2004. Felsenmeer persistence under non-erosive ice in the Torngat and Kaumajet mountains, Quebec and Labrador, as determined by soil weathering and cosmogenic nuclide exposure dating. Can. J. Earth Sci. 41 (1), 19–38. https://doi.org/10.1139/e03-072.

Möller, P., Anjar, J., Murray, A.S., 2013a. An OSL-dated sediment sequence at Idre, west-central Sweden, indicates ice-free conditions in MIS 3. Boreas 42 (1), 25–42. https://doi.org/10.1111/j.1502-3885.2012.00284.x.

Möller, P., Östlund, O., Barnekow, L., Sandgren, P., Palmbo, F., Willerslev, E., 2013b. Living at the margin of the retreating fennoscandian ice sheet: the early mesolithic sites at Aareavaara, northernmost Sweden. Holocene 23 (1), 104–116. https://doi.org/10.1177/0959683612455546.

Nishiizumi, K., 2004. Preparation of 26Al AMS standards. Nucl. Instrum. Methods Phys. Res. Sect. B Beam Interact. Mater. Atoms 223–224, 388–392. https://doi.org/10.1016/j.nimb.2004.04.075.

Olsen, L., Sveian, H., Ottesen, D., Rise, L., 2013. Quaternary glacial, interglacial and interstadial deposits of Norway and adjacent onshore and offshore areas. Quaternary Geology of Norway, Geological Survey of Norway Special Publication 13, 79–144.

Patton, H., Hubbard, A., Heyman, J., Alexandropoulou, N., Lasabuda, A.P.E., Stroeven, A.P., Hall, A.M., Winsborrow, M., Sugden, D.E., Kleman, J., Andreassen, K., 2022. The extreme yet transient nature of glacial erosion. Nat. Commun. 13 (1), 7377. https://doi.org/10.1038/s41467-022-35072-0.

Peterson Becher, G., Mikko, H., Smith, C., Öhrling, C., Ransed, G., Goodfellow, B., 2022. The Geomorphological Imprint and Implications of a 'new' Ice Margin in Central Sweden.

Phillips, W.M., Hall, A.M., Mottram, R., Fifield, L.K., Sugden, D.E., 2006. Cosmogenic 10Be and 26Al exposure ages of tors and erratics, Cairngorm Mountains, Scotland: timescales for the development of a classic landscape of selective linear glacial erosion. Geomorphology 73 (3), 222–245. https://doi.org/10.1016/j.geomorph.2005.06.009.

Plikk, A., Helmens, K.F., Fernández-Fernández, M., Kylander, M., Löwemark, L., Risberg, J., Salonen, J.S., Väliranta, M., Weckström, J., 2016. Development of an Eemian (MIS 5e) Interglacial palaeolake at Sokli (N Finland) inferred using multiple proxies. Palaeogeogr. Palaeoclimatol. Palaeoecol. 463, 11–26. https://doi.org/10.1016/j.palaeo.2016.09.008.

Porter, C., Howat, I., Noh, M.-J., Husby, E., Khuvis, S., Danish, E., Tomko, K., Gardiner, J., Negrete, A., Yadav, B., Klassen, J., Kelleher, C., Cloutier, M., Bakker, J., Enos, J., Arnold, G., Bauer, G., Morin, P., 2023. ArcticDEM - mosaics, version 4.1. Harvard Dataverse. https://doi.org/10.7910/DVN/3VDC4W.

Raab, G., Martin, A.P., Norton, K.P., Christl, M., Scarciglia, F., Egli, M., 2021. Complex patterns of schist tor exposure and surface uplift, Otago (New Zealand). Geomorphology 389, 107849. https://doi.org/10.1016/j.geomorph.2021.107849.

Raab, G., Scarciglia, F., Norton, K., Dahms, D., Brandová, D., de Castro Portes, R., Christl, M., Ketterer, M.E., Ruppli, A., Egli, M., 2018. Denudation variability of the Sila Massif upland (Italy) from decades to millennia using 10Be and 239+240Pu. Land Degrad. Dev. 29 (10), 3736–3752. https://doi.org/10.1002/ldr.3120.

Raymo, M.E., Ruddiman, W.F., Backman, J., Clement, B.M., Martinson, D.G., 1989. Late Pliocene variation in northern hemisphere ice sheets and North Atlantic deep water circulation. Paleoceanography 4 (4), 413–446. https://doi.org/10.1029/PA004i004p00413.

Robertsson, A.-M., 1997. Reinvestigation of the interglacial pollen flora at Leveäniemi, Swedish Lapland. Boreas 26 (2), 81–89. https://doi.org/10.1111/j.1502-3885.1997.tb00654.x.

Ruddiman, W.F., Raymo, M.E., Martinson, D.G., Clement, B.M., Backman, J., 1989. Pleistocene evolution: northern hemisphere ice sheets and north atlantic ocean. Paleoceanography 4 (4), 353–412. https://doi.org/10.1029/PA004i004p00353.

Salonen, V.-P., Moreau, J., Hyttinen, O., Eskola, K.O., 2014. Mid-weichselian interstadial in kolari, western Finnish lapland. Boreas 43 (3), 627–638. https://doi.org/10.1111/bor.12060.

Sarala, P., 2005. Landform development during the weichselian glaciation in peräpohjola, Finland. Quaternary studies in the northern and Arctic regions of Finland 40, 59–65.

Sarala, P., Pihlaja, J., Putkinen, N., Murray, A., 2010. Composition and origin of the Middle Weichselian interstadial deposit in Veskoniemi, northern Finland. Est. J. Earth Sci. 59 (2), 117–124.

Sarala, P., Väliranta, M., Eskola, T., Vaikutiené, G., 2016. First physical evidence for forested environment in the Arctic during MIS 3. Sci. Rep. 6 (1). https://doi.org/10.1038/srep29054. Article 1.

Schaefer, J.M., Finkel, R.C., Balco, G., Alley, R.B., Caffee, M.W., Briner, J.P., Young, N.E., Gow, A.J., Schwartz, R., 2016. Greenland was nearly ice-free for extended periods during the Pleistocene. Nature 540 (7632), 252–255. https://doi.org/10.1038/nature20146.

Siddall, M., Rohling, E.J., Thompson, W.G., Waelbroeck, C., 2008. Marine isotope stage 3 sea level fluctuations: data synthesis and new outlook. Rev. Geophys. 46 (4). https://doi.org/10.1029/2007RG000226.

Skov, D.S., Andersen, J.L., Olsen, J., Jacobsen, B.H., Knudsen, M.F., Jansen, J.D., Larsen, N.K., Egholm, D.L., 2020. Constraints from cosmogenic nuclides on the glaciation and erosion history of Dove Bugt, northeast Greenland. GSA Bulletin 132 (11–12), 2282–2294. https://doi.org/10.1130/B35410.1.

Small, E.E., Anderson, R.S., Repka, J.L., Finkel, R., 1997. Erosion rates of alpine bedrock summit surfaces deduced from in situ 10Be and 26Al. Earth Planet Sci. Lett. 150 (3), 413–425. https://doi.org/10.1016/S0012-821X(97)00092-7.

Spielhagen, R.F., Baumann, K.-H., Erlenkeuser, H., Nowaczyk, N.R., Nørgaard-Pedersen, N., Vogt, C., Weiel, D., 2004. Arctic Ocean deep-sea record of northern Eurasian ice sheet history. Quat. Sci. Rev. 23 (11), 1455–1483. https://doi.org/10.1016/j.quascirev.2003.12.015.

Stone, J.O., 2000. Air pressure and cosmogenic isotope production. J. Geophys. Res. Solid Earth 105 (B10), 23753–23759. https://doi.org/10.1029/2000JB900181.

Stroeven, A.P., Fabel, D., Hättestrand, C., Harbor, J., 2002. A relict landscape in the centre of Fennoscandian glaciation: cosmogenic radionuclide evidence of tors preserved through multiple glacial cycles. Geomorphology 44 (1), 145–154. https://doi.org/10.1016/S0169-555X(01)00150-7.

Stroeven, A.P., Fabel, D., Margold, M., Clague, J.J., Xu, S., 2014. Investigating absolute chronologies of glacial advances in the NW sector of the Cordilleran Ice Sheet with terrestrial in situ cosmogenic nuclides. Quat. Sci. Rev. 92, 429–443. https://doi.org/10.1016/j.quascirev.2013.09.026.

Stroeven, A.P., Harbor, J., Fabel, D., Kleman, J., Hättestrand, C., Elmore, D., Fink, D., Fredin, O., 2006. Slow, patchy landscape evolution in northern Sweden despite repeated ice-sheet glaciation. In: Willett, S.D., Hovius, N., Brandon, M.T., Fisher, D. M. (Eds.), Tectonics, Climate, and Landscape Evolution, vol. 398. Geological Society of America. https://doi.org/10.1130/2006.2398(24.

Stroeven, A.P., Hättestrand, C., Kleman, J., Heyman, J., Fabel, D., Fredin, O., Goodfellow, B.W., Harbor, J.M., Jansen, J.D., Olsen, L., Caffee, M.W., Fink, D., Lundqvist, J., Rosqvist, G.C., Strömberg, B., Jansson, K.N., 2016. Deglaciation of Fennoscandia. Quat. Sci. Rev. 147, 91–121. https://doi.org/10.1016/j.quascirev.2015.09.016.

Stroeven, A.P., Heyman, J., Fabel, D., Björck, S., Caffee, M.W., Fredin, O., Harbor, J.M., 2015. A new Scandinavian reference 10Be production rate. Quat. Geochronol. 29, 104–115. https://doi.org/10.1016/j.quageo.2015.06.011.

Sugden, D.E., Hein, A.S., Woodward, J., Marrero, S.M., Rodés, Á., Dunning, S.A., Stuart, F.M., Freeman, S.P.H.T., Winter, K., Westoby, M.J., 2017. The million-year evolution of the glacial trimline in the southernmost Ellsworth Mountains, Antarctica. Earth Planet Sci. Lett. 469, 42–52. https://doi.org/10.1016/j.epsl.2017.04.006.

Sutinen, R., Middleton, M., 2021. Porttipahta end moraine in Finnish Lapland is constrained to Early Weichselian (MIS 5d, Herning stadial). Geomorphology 393, 107942. https://doi.org/10.1016/j.geomorph.2021.107942.

Svendsen, J.I., Alexanderson, H., Astakhov, V.I., Demidov, I., Dowdeswell, J.A., Funder, S., Gataullin, V., Henriksen, M., Hjort, C., Houmark-Nielsen, M., Hubberten, H.W., Ingólfsson, Ó., Jakobsson, M., Kjær, K.H., Larsen, E., Lokrantz, H., Lunkka, J.P., Lysså, A., Mangerud, J., et al., 2004. Late Quaternary ice sheet history of northern Eurasia. Quat. Sci. Rev. 23 (11), 1229–1271. https://doi.org/10.1016/j.quascirev.2003.12.008.

Ukkonen, P., Lunkka, J.P., Jungner, H., Donner, J., 1999. New radiocarbon dates from Finnish mammoths indicating large ice-free areas in Fennoscandia during the Middle Weichselian. J. Quat. Sci. 14 (7), 711–714. https://doi.org/10.1002/(SICI)1099-1417(199912)14:7<711::AID-JQS506>3.0.CO;2-E.

Väliranta, M., Birks, H.H., Helmens, K., Engels, S., Piirainen, M., 2009. Early Weichselian interstadial (MIS 5c) summer temperatures were higher than today in northern Fennoscandia. Quat. Sci. Rev. 28 (9), 777–782. https://doi.org/10.1016/j.quascirev.2009.01.004.

Waller, R.I., Murton, J.B., Kristensen, L., 2012. Glacier–permafrost interactions: processes, products and glaciological implications. Sediment. Geol. 255–256, 1–28. https://doi.org/10.1016/j.sedgeo.2012.02.005.

Winograd, I.J., 2001. The magnitude and proximate cause of ice-sheet growth since 35,000 yr B.P. Quaternary Research 56 (3), 299–307. https://doi.org/10.1006/qres.2001.2272.